Leptin brain entry via a tanycytic LepR–EGFR shuttle controls lipid metabolism and pancreas function

Manon Duquenne, Cintia Folgueira, Cyril Bourouh, Marion Millet, Anisia Silva, Jérôme Clasadonte, Monica Imbernon, Daniela Fernandois, Ines Martinez-Corral, Soumya Kusumakshi, et al.

Submission: April 2, 2021
Nature Metabolism
Research Article

Leptin enters the brain through a LepR:EGFR shuttle in tanycytes to regulate peripheral lipogenesis and pancreatic β-cell function

Manon Duquenne[1], Cintia Folgueira[2#], Cyril Bourrouh[3#], Marion Millet[4,#], Anisia Silva[5#], Jérôme Clasadonte[1#], Monica Imbernon[1], Daniela Fernandois[1], Ines Martinez-Corral[1], Soumya Kusumakshi[6], Emilie Caron[1], S. Rasika[1], Eleonora Deliglia[1], Nathalie Jouy[1,12], Asturo Oishi[5], Massimiliano Mazzone[7], Eric Trinquet[8], Jan Tavernier[9], Young-Bum Kim[11], Stéphane Ory[4], Ralf Jockers[5], Markus Schwaninger[10], Ulrich Boehm[6], Ruben Nogueiras[2], Jean-Sébastien Annicotte[3], Stéphane Gasman[4&], Julie Dam[5&], Vincent Prévot[1&*]

[1] Univ. Lille, Inserm, CHU Lille, Laboratory of Development and Plasticity of the Neuroendocrine Brain, Lille Neuroscience & Cognition, UMR_S1172, EGID, DISTALZ, F-59000 Lille, France
[2] CIMUS, Universidade de Santiago de Compostela-Instituto de Investigación Sanitaria, Santiago de Compostela, 15782, Spain- CIBER Fisiopatología de la Obesidad y Nutrición (CIBERobn), 15706, Spain
[3] Univ. Lille, Inserm, CHU Lille, Institut Pasteur de Lille, CNRS, U1283 - UMR 8199 - EGID, F-59000 Lille, France
[4] Centre National de la Recherche Scientifique, Université de Strasbourg, Institut des Neurosciences Cellulaires et Intégratives, F-67000 Strasbourg, France.
[5] Institut Cochin, Inserm U1016, CNRS UMR 8104, University Paris Descartes, Sorbonne Paris Cité, Paris, France
[6] Experimental Pharmacology, Center for Molecular Signaling (PZMS), Saarland University School of Medicine, 66421, Homburg, Germany
[7] Laboratory of Tumor Inflammation and Angiogenesis, Center for Cancer Biology, VIB, Department of Oncology, KU Leuven, Leuven, B3000, Belgium
[8] Cisbio Bioassays, Parc Technologique Marcel Boiteux, BP84175, F-30200 Codolet, France
[9] VIB-UGent Center for Medical Biotechnology, Gent, Belgium.
[10] Institute for Experimental and Clinical Pharmacology and Toxicology, University of Lübeck, Lübeck, Germany
[11] Division of Endocrinology, Diabetes, and Metabolism, Beth Israel Deaconess Medical Center and Harvard Medical School, Boston, MA, USA.
[12] Flow core Facility, BioImaging Center of Lille, campus HU, UMS2014-US41, F-59000 Lille, France

[#] These authors contributed equally to this work
[&] These authors jointly supervised this work

Running Title: Tanycytes are conduits for peripheral metabolic signals into the brain

* Corresponding author: Vincent Prevot, Ph.D., Inserm 1172, Bâtiment Biserte,
Place de Verdun, 59045 Lille Cedex, France
Tel : +33 612-90-38-76
Fax : +33 320-53-85-62
E-mail : vincent.prevot@inserm.fr

Number of text pages: 53
Number of figures: 7
Number of Supplementary Figures: 7
Number of tables: 0
Number of words (abstract): 150
Number of words (Text): 7290

SUMMARY

Metabolic health depends on the brain's ability to control food intake and nutrient use versus storage, processes that require peripheral signals such as the adipocyte-derived hormone, leptin, to cross brain barriers and mobilize regulatory circuits. We have previously shown that hypothalamic tanycytes shuttle leptin into the brain to reach target neurons. Here, using multiple complementary models, we show that tanycytes express functional leptin receptor (LepRb), respond to leptin by triggering Ca2+ waves and target-protein phosphorylation, and that their transcytotic transport of leptin requires the activation of a LepR:EGFR complex by leptin and EGF sequentially. Selectively deleting LepR in tanycytes blocks leptin entry into the brain, inducing not only increased food intake and lipogenesis but glucose intolerance through attenuated insulin secretion by pancreatic β-cells, possibly via altered sympathetic nervous tone. Tanycytic LepRb:EGFR-mediated transport of leptin could thus be crucial to the pathophysiology of diabetes in addition to obesity, with therapeutic implications.

INTRODUCTION

Type 2 diabetes (T2D) is a common multigenic disorder affecting almost 10% of the world's population [1]. However, the characteristics of this disorder do not appear to be homogeneous across the globe. In Asia, for example, TD2 develops in a much shorter time, in a younger age group, and in people with a much lower body-mass index (BMI) than in patients from other parts of the globe [2]. In addition, while Asian population studies suggest that a decrease in insulin production by β-cells is crucial for the development of diabetes, impaired insulin sensitivity, i.e. the ability to modulate glucose levels in response to circulating insulin, appears to be a prerequisite for incident diabetes in other ethnicities, including Europeans [2,3].

Leptin is a 16-kDa peptide hormone produced by adipocytes. It functions as an afferent signal in a negative feedback loop that not only controls feeding and maintains energy homeostasis [4-9], but also regulates glucose metabolism [10,11] and substrate fluxes [12,13] by activating leptin receptor (LepR) signaling in the brain. How circulating leptin is transported into the central nervous system to reach its target neurons remains an enigma. However, an increasing body of evidence points to the median eminence, a circumventricular organ in the basal hypothalamus adjacent to the arcuate nucleus (ARH), as a key entrance point for leptin into the metabolic brain [14-16].

By virtue of the fenestrated or porous endothelium of the underlying pituitary portal blood vessels, which replaces a traditional blood-brain barrier (BBB), the median eminence acts as a brain window at which circulating signals, including metabolic hormones, may enter the brain by passive diffusion [17,18]. Among the neuronal populations responsive to metabolic hormones in this region, those of the ventromedial ARH (vmARH) [17,19] and neurons that extend dendrites into the median eminence can directly sense this local blood-borne information [20]. However, the passive diffusion of metabolic signals into the median eminence is limited in extent [17,19], and tanycytes, a specialized glial cell type lining the floor of the third ventricle (3V), form a blood-cerebrospinal-fluid (CSF) barrier that prevents these circulating metabolic signals from reaching deeper hypothalamic structures through the CSF [14-16]. Consequently, in order to reach more distant targets such as neurons of the dorsomedial ARH (dmARH), these signals require an active transport mechanism to cross the tanycytic blood-CSF barrier [21,22].

In a previous study, we have shown that tanycytes, whose end-feet contact the fenestrated capillaries of the median eminence, themselves internalize and shuttle blood-borne leptin

extravasating from these fenestrations into the CSF, in an ERK-dependent manner [23]. However, the putative involvement of LepR in this transcytotic transport process has remained unclear, with some authors questioning the expression of LepR by tanycytes [24,25].

Here, by employing multiple *in vitro* and *in vivo* approaches and several mouse models, we demonstrate that tanycytes do indeed express functional LepR, and that this LepR expression is required for the transcytotic transport of peripheral leptin into the CSF, a process that appears to play a vital role in the central control of pancreatic β-cell function, lipid accumulation and subsequent glucose homeostasis.

RESULTS

LepR is expressed and active in tanycytes of the median eminence

In order to verify the expression of LepR by median eminence and ARH tanycytes, we first used the powerful RNAscope approach with probes targeting the long and short forms of LepR, LepRb and LepRa, respectively. Interestingly, while both isoforms were present in tanycytic cell bodies lining the walls of the 3V, this expression was relatively weak compared to the overwhelmingly high expression seen in leptin-responsive neurons of the ARH, providing an explanation for the failure of other, less sensitive, methods to detect tanycytic LepR expression without resorting to the isolation of these cells (Supplementary Figure 1A). We therefore searched for other tools such as novel antibodies capable of reliably detecting LepR protein in order to confirm its presence in median eminence tanycytes. We characterized the recently described biologically active allosteric antibody XPA, which was developed to target mouse LepR [26]. Using isolated parts/fragments of the LepR extracellular domain (ECD), we found that the epitope specifically targeted by XPA lies in the cytokine receptor homology 1 (CRH1) domain of mouse LepR (Figure 1A; Supplementary Figure 1B), outside the orthosteric leptin-binding site of the CRH2 domain (Figure 1A, 1B). The use of LepR BRET biosensors indicated that XPA was capable of inducing conformational changes and the oligomerization of LepR, even though these changes were different from the ones promoted by the natural ligand (Figure 1C). Similarly to leptin (50nM), treatment with 100nM XPA consistently triggered STAT3 signaling in HEK293, N46, HeLa and CHO cells transfected with LepRb (Figure 1D; Supplementary Figure 1C), as well as ERK signaling in HEK293 cells (Figure 1D). XPA also induced the phosphorylation of STAT3 in primary cultures of tanycytes (Figure 1E), which we have previously shown to express LepR and to internalize

fluorescently labeled leptin *in vitro* [23]. This indicates that, rather than simply being a passive marker of LepR protein expression, XPA is also a vital marker for activated and internalized LepR. Accordingly, a 5 min co-application of fluorescent leptin (125nM) and fluorescent XPA (30nM) to primary tanycyte cultures showed that 100% of the cells that internalized fluorescent leptin also internalized fluorescent XPA, and that 50 to 60% of the endocytosed leptin colocalized with XPA *in vitro* (Figure 1F), indicating that these cells expressed LepR and internalized it in response to leptin binding. To confirm that tanycytes also express LepR *in vivo*, we intravenously administered XPA (2 nmol/animal) or vehicle to mice 2 min before sacrifice. At this short interval, XPA was seen to colocalize with the vimentin-immunoreactive cell bodies and processes of tanycytes arching down to the fenestrated capillary plexus of the median eminence (Figure 1G).

In our quest for further indisputable evidence of LepR expression and function in median eminence tanycytes, we assessed whether tanycytes in living brain slices could respond to leptin and initiate Ca^{2+} signaling, as hypothalamic neurons do [27,28]. To selectively target tanycytes, we generated mice expressing the GCamp3 calcium biosensor under the control of the Trmp5 promoter, which is selectively expressed in tanycytes in the median eminence and present in the majority of this cell population (Figure 1H) [29], by crossing *Trmp5*::*Cre* mice with those allowing Cre-dependent expression of GCamp3. Puffing 6 μM leptin onto the ventricular wall of brain slices against the flow of perfusion resulted in a $[Ca^{2+}]_i$ increase in the cell bodies of median eminence tanycytes, as seen using live imaging (Figure 1H, and 1I). A bath-application of 6 μM of the point-mutated leptin LAN (L39A/D40A/F41A), which acts as a competitive antagonist by binding LepR but blocking its activity [30], prior to puffing leptin onto tanycytes inhibited the leptin-induced $[Ca^{2+}]_i$ increase in these cells (Figure 1I, and 1K), suggesting that LepR activation is required for this signaling cascade. To further test the actual involvement of LepR in this process, we generated mice in which LepR was selectively knocked out in cells expressing the *Trmp5* promoter. In these *Trmp5*::*Cre*; $LepR^{loxP/loxP}$; $GCamp3^{loxP/STOP/loxP}$ mice ($Gcamp3^{Trmp5}$; $LepR^{Trmp5KO}$ mice), puffs of leptin failed to promote any change in $[Ca^{2+}]_i$ in tanycytes (Figure 1J, and 1K). However, puffs of 10 mM ATP, a well-known and potent activator of calcium waves in tanycytes [31,32], readily elevated $[Ca^{2+}]_i$ in both LAN-treated and mutated brain slices, showing the viability of the cells (Figure 1L, Supplementary Figure 2). Together, these data unequivocally show that tanycytes *in vivo* express active LepR, which mediates leptin-induced changes in $[Ca^{2+}]_i$.

EGFR-mediated LepRb signaling is required for the transcellular trafficking of leptin in tanycytes

To characterize the mechanism by which tanycytes transport blood-borne leptin into the CSF and the rest of the hypothalamus, we next studied the transcytotic route followed by fluorescent leptin using primary cultures of tanycytes. As early as 2 min after the internalization of fluorescent bioactive leptin, the fluorescent signal was detected in EEA1-immunoreactive early endosomes (Figure 2A), where it accumulated for the first 10 min. The fluorescent leptin then exited this subcellular compartment, as indicated by the subsequent decrease in intensity and extinction of fluorescence over time (Figure 2B, Figure 2C, Supplementary Figure 3A), along with leptin release into the culture medium (Figure 2D). Similarly, fluorescent LAN, which binds to but is unable to activate LepR, was also seen to be internalized (Supplementary Figure 3B) and to reach early endosomes (Supplementary Figure 3D). However, the overall intensity of LAN fluorescence inside the cell remained constant over time (Supplementary Figure 3B), and LAN was seen to remain sequestered in EEA1-immunoreactive compartments (Figure 2E, Supplementary Figure 3C-D), suggesting that, in contrast to bioactive leptin, captured LAN could not be released from tanycytes. These results suggest that LepR signaling is not required for leptin uptake, but is required for internalized leptin to complete its transcytotic route across tanycytes into the CSF.

Next, since this transcytosis could be mediated by the leptin signaling cascade, characterized by the rapid activation of a series of tyrosine kinases (TK) and serine/threonine protein kinases (STK), we performed kinome profiling to explore differential global kinase activity in tanycytes in the presence or absence of 125nM leptin for 2, 5, 10 and 15 min. We used the PamGene array, which consists of 140 immobilized tyrosine- and serine/threonine-containing peptides that are the targets of most known kinases (TK and STK PamChips). Peptides whose phosphorylation varied significantly between control and leptin-treated primary tanycytes indicated the putative activation of specific kinases in response to leptin. This kinase analysis revealed the significant activation of the EGFR pathway 2 min after leptin treatment (Figure 2F) and of MAP kinases, including ERK, 2 15 min after leptin treatment (Supplementary Figure 3E). We have previously reported that ERK activation is required for the release of leptin internalized by tanycytes *in vitro,* and that the alteration of blood-borne leptin shuttling into the hypothalamus in diet-induced obese mice can be rescued by activating ERK using potent

inducers such as EGF [23]. Here, the novel and unexpected finding that EGFR itself is *trans*-activated by leptin in tanycytes suggests a possible molecular pathway underlying our previous observations.

In vivo, EGFR immunoreactivity was detected both in the cell bodies of tanycytes lining the walls and floor of the 3V and in their distal processes, which contact fenestrated capillaries at the pial surface of the brain in the external zone of the median eminence (Supplementary Figure 4A). Polymerase ligation assays using XPA demonstrated the extensive physical interaction of EGFR and LepRb in both cellular compartments, a phenomenon that is blunted in *Trmp5*::*Cre*; *LepR*$^{loxP/loxP}$ mice (Figure 2G), suggesting that LepRb:EGFR signaling in tanycytic end-feet may play a role in the transcellular transport of circulating leptin once it is captured from the bloodstream.

We then explored this interaction between EGFR and LepR signaling. Co-transfection experiments in HEK293 cells confirmed that EGFR was immunoprecipitated with LepR, suggesting, intriguingly, that the two receptors could physically interact with each other even in the absence of a ligand (Figure 2H). To study the effect of ligand binding on this interaction, we next used Time-Resolved Fluorescence Resonance Energy Transfer (TR-FRET) in living HEK293 cells to investigate the proximity between leptin and EGF and their cognate receptors within the LepR:EGFR complex (Supplementary Figure 3F). Taking advantage of targeted fluorescently-labeled SNAP receptors (energy donor, Terbium (**Tb**)) and ligands (labeled with the energy acceptor, **d2**), TR-FRET enables the demonstration of the proximity of a ligand at a distance of 10 nm or less to a specific and unique receptor within a heteromeric receptor complex [33]. Because leptin does not bind to EGFR, the incubation of fluorescent leptin-d2 even at high concentrations with fluorescently labeled SNAP-EGFR did not lead to any TR-FRET signal (Figure 2I, Supplementary Figure 3F). However, the co-expression of unlabeled LepR in fluorescent SNAP-EGFR-expressing cells in the presence of leptin-d2 gave rise to a significant and specific TR-FRET signal, demonstrating the close proximity between SNAP-EGFR, LepR and leptin-d2 (Figure 2I, Supplementary Figure 3F). This binding of leptin-d2 to the SNAP-EGFR:LepR complex was seen to increase and to reach saturation in a concentration-dependent manner, with an affinity (K_D(SNAP-EGFR:LepRb) = 0.42 [0.26-0.49] nM) similar to the affinity of leptin binding to isolated LepR [34] (Figure 2I). EGF binding to EGFR did not modify the affinity of leptin binding to the LepR:EGFR complex (Figure 2I), but the significantly higher Bmax of the saturation curve indicates that it likely induced a conformational change in LepR within the molecular complex (Figure 2I; Supplementary Figure 3G). Similarly, cells expressing EGFR and fluorescent SNAP-LepR

that were stimulated by EGF-d2 (Supplementary Figure 3H) were seen to emit a specific TR-FRET signal, reflecting the interaction between SNAP-LepR:EGFR:EGF-d2 (Supplementary Figure 3I). A weak TR-FRET signal detected between SNAP-LepR and EGF-d2 in the absence of heterologous EGFR may have arisen from a weak interaction between SNAP-LepR and endogenous EGFR. As suggested by the model fitting of the saturation curve, EGF-d2 interacted with EGFR within the LepR:EGFR complex with the same affinity (K_D(SNAP-LepRb:EGFR) = 2.1 [1.6-2.5] nM) as with isolated EGFR alone (K_D(SNAP-EGFR) = 3.2 [2.4-3.7]) (Supplementary Figure 3J). In line with the binding of leptin-d2 or EGF-d2 to their cognate receptors within the complex, the proximity of fluorescent leptin-Tb (energy donor) to EGF-d2 (energy acceptor) was only detected when both LepR and EGFR were co-expressed (Supplementary Figure 3K, 3L), suggesting the formation of a quaternary complex, Leptin:LepR:EGFR:EGF, in these cells.

In isolated tanycytes, combined treatment with leptin and EGF enhanced EGFR and ERK phosphorylation, supporting the intricate collaboration between these two receptors at the level of the tanycytic ERK signaling pathway (Figure 2J). Accordingly, EGF potentiated the leptin:LepR activation of the ERK signaling pathway in HEK293T cells, a reaction that was blunted by pre-treating the cells with the EGFR kinase inhibitor, AG1478 (Figure 2K). Conversely, the inhibition of MEK1/2, the upstream activators of ERK, using U0126 led to the accumulation of fluorescent leptin in EAA1-immunoreactive early endosomes in tanycytes and blunted its release (Figure 2D), thus phenocopying the behavior of fluorescent LAN, which does not activate LepR, after its internalization by tanycytes (Figure 2E, Supplementary Figure 3B, 3C, 3D). We next verified whether this lack of LAN release from the early endosome compartment in tanycytes could be bypassed by directly activating the EGFR-ERK signaling pathway. EGF treatment (1.5nM) strikingly restored the trafficking of fluorescent LAN downstream of early endosomes (Figure 2E) and its probable release by tanycytes, suggesting that EGFR activation occurs downstream of LepR activation (Supplementary Figure 3C). Together, these data indicate that the transcytosis of leptin by tanycytes, which allows it to reach the CSF and distant hypothalamic tissues, requires LepR-EGFR-ERK signaling.

Mice lacking LepR-EGFR signaling in adult tanycytes show increased fat mass gain linked to restricted access of blood-borne leptin to the hypothalamus

To examine the functional role of LepR expression in adult tanycytes, we used the injection of the TAT-Cre recombinant protein into the 3V of *LepR*$^{loxP/loxP}$ mice. The use of *tdTomato*$^{loxP\text{-}STOP\text{-}loxP}$ reporter mice revealed that 2 µl TAT-Cre infusion into the 3V (1.27 µg/µl over 15 min) caused genetic recombination in about 60% of the tanycytes of the median eminence (Supplementary Figure 5A and 5B), but not in tanycytes of the area postrema, another circumventricular organ in the brainstem involved in the regulation of energy homeostasis [35] (Supplementary Figure 5C). In contrast, TAT-Cre infusion into the fourth ventricle (4V) was seen to target both median eminence and area postrema tanycytes (Supplementary Figure 5C), while TAT-Cre infusion into the lateral ventricle was ineffective in inducing Tomato expression in median eminence tanycytes (Supplementary Figure 5A - 5B). FACS isolation of Tomato-positive ependymal cells from microdissected dorsal and ventral aspects of the 3V, which are enriched in ciliated ependymal cells and tanycytes, respectively (Supplementary Figure 5D), showed that LepR expression was readily detected by real-time PCR in the tanycyte-enriched population, but not in classical ependymal cells (Supplementary Figure 5E). Accordingly, FACS isolation of Tomato-positive median eminence tanycytes after the infusion of TAT-Cre into the 3V of *tdTomato*$^{loxP\text{-}STOP\text{-}loxP}$; *LepR*$^{loxP/loxP}$ mice (Figure 3A) showed that the expression of transcripts encoding both the short forms of LepR as well as LepRb was significantly diminished in these cells, when compared to Tomato-positive tanycytes from *tdTomato*^{Tan}; *LepR*$^{+/+}$mice (Figure 3B and 3C). Interestingly, the transcript of *Socs3*, a known leptin-responsive transcriptional target [36], was also found to be downregulated in Tomato-positive cells from *tdTomato*^{Tan}; *LepR*^{TanKO} mice (Figure 3D). Importantly, *LepR* and *Socs3* mRNA levels were not downregulated in Tomato-negative cells (Figure 3B-3D). The TAT-Cre-mediated loss of *LepR* expression in tanycytes was also accompanied by a dramatic decrease in the PLA signal reporting the physical association between LepRb and EGFR (Figure 2G), as seen in *Trmp5*::*Cre*; *LepR*$^{loxP/loxP}$ mice.

Interestingly, mice lacking LepR in tanycytes of the median eminence were seen to eat more (Supplementary Figure 6A), specifically in the morning after lights-on (Figure 3E). They also gained significantly more weight (Figure 3F) than both vehicle-injected control littermates with normal tanycytic LepR expression and TAT-Cre-injected heterozygous mice (*LepR*^{TanHet}). This weight gain was associated with a 3-fold increase in fat mass 12 weeks after *LepR* was knocked out in tanycytes (Figure 3G), with a concomitant loss of lean mass (Figure 3H) such that the net gain in body mass remained moderate (Supplementary Figure 6B). At 12 weeks post-TAT-Cre injection, *LepR*^{TanKO} mice

showed a significant increase in visceral (Figure 3I), but not subcutaneous fat mass (Figure 3J) when compared to vehicle-injected *LepR*$^{loxP/loxP}$ littermates. Surprisingly, this weight gain was independent of hyperphagia, since *LepR*^{TanKO} mice pair-fed with controls gained the same weight as *LepR*^{TanKO} mice fed *ad libitum* (Figure 3K and 3L). To characterize the reason for this change in body weight, we monitored these mice using an indirect calorimetry system. Weight gain in *LepR*^{TanKO} mice was associated with an increased respiratory exchange ratio (RER) during the light phase both at 4 weeks (Supplementary Figure 6A2) and 12 weeks after TAT-Cre injection (Figure 3M and 3N), a phenomenon that was conserved under the pair-fed condition (Figure 3K), in which *LepR*^{TanKO} mice kept gaining more weight than *LepR*$^{loxP/loxP}$ littermates (Figure 3L), even though energy expenditure (Supplementary Figure 6A3 and 6C) and locomotor activity (Supplementary Figure 6A4 and 6D) remained unchanged. These phenomena were reproduced when tanycytes *in vivo* were transduced with a viral vector expressing Cre under the control of the tanycyte-specific *Dio2* promoter [31], as an alternative to TAT-Cre infusion into the 3V (Supplementary Figure 6A5-A8).

Interestingly, in accordance with the marked increase in fat mass, circulating levels of leptin were seen to be increased as early as 4 weeks after the TAT-Cre-mediated *LepR* deletion in tanycytes (Figure 3O). Taking into account the close relationship between LepR and EGFR and the likely *trans*-activation of LepR to some extent by endogenous EGF (Figure 2, Supplementary Figure 3), we therefore also measured EGF levels in the blood of *LepR*^{TanKO} mice, to determine whether the lack of LepR signaling in these mice would give rise to compensatory changes in the EGF-EGFR signaling pathway. Interestingly, we found that EGF levels, which we could readily detect in the circulation, were increased in *LepR*^{TanKO} mice (Figure 3P). However, EGF levels were unchanged in wild-type mice given a high-fat diet for 8 weeks as compared to chow-fed controls (Figure 3Q), suggesting that the increase in EGF levels in *LepR*^{TanKO} mice were not related to the higher circulating leptin levels observed in these animals per se (Figure 3O), but rather to central phenomena linked to deficient LepR signaling.

Increased food intake after overnight feeding (Figure 3E) despite elevated adiposity (Figure 3G and 3I) and circulating levels of leptin in *LepR*^{TanKO} mice (Figure 3O) further raised the possibility that these animals could be developing hypothalamic resistance to circulating leptin, linked to defective leptin transport across the BBB into the CSF by tanycytes, as seen at early stages of diet-induced obesity in various animal models [23,37]. First, to confirm that this phenomenon occurs under physiological

conditions, we assessed endogenous STAT3 activation in the ARH, which has previously been shown to be linked to endogenous LepR activation [22,38], at lights-on after overnight feeding, when circulating leptin levels are at their highest [39]. While the number of P-STAT3-immunoreactive cells lying outside the BBB in the vmARH was seen to be unaffected in *LepR*^{TanKO} mice (Supplementary Figure 7A and 7B), the number of P-STAT-3 immunoreactive cells in the dmARH was diminished by about 30% in these mutant mice when compared to *LepR*$^{loxP/loxP}$ control littermates (Supplementary Figure 7A and 7C). We then assessed the ability of exogenous leptin to activate leptin-sensitive hypothalamic neurons 15 min after an intraperitoneal (i.p.) bolus injection. While leptin-induced P-STAT3 activation was unaffected in the vmARH (Figure 4A and 4B), it was still significantly hampered in the dmARH of *LepR*^{TanKO} mice when compared to *LepR*$^{loxP/loxP}$ mice (Figure 4A and 4C). To determine how this decreased access to peripheral leptin could impact the neuronal populations of the ARH involved in the control of body homeostasis, we analyzed the expression of several key leptin-regulated transcripts by q-PCR. Figure 4D shows that, in *LepR*^{TanKO} mice, transcripts coding for the melanocortin receptor antagonist *Agrp* were significantly induced, whereas *Socs3* mRNA levels were downregulated. Next, we subjected *LepR*^{TanKO} mice as well as their control littermates to an i.p. or intracerebroventricular (i.c.v.) injection of exogenous leptin and measured food intake 24h (Figure 4E). While exogenous leptin injected i.c.v. directly into the CSF was equally efficient in reducing feeding in both groups of mice, *LepR*^{TanKO} mice, in contrast to *LepR*$^{loxP/loxP}$ mice, were unable to respond to exogenous leptin injected i.p. by decreasing food intake (Figure 4E), suggesting once again that tanycytic LepR is necessary for peripheral leptin to reach leptin-sensitive neurons not in the immediate vicinity of fenestrated vessels in the median eminence. Finally, we further verified that the decreased response to peripheral leptin in *LepR*^{TanKO} mice was due to an alteration in the LepR-dependent tanycytic transport of blood-borne leptin into the hypothalamus by implanting microdialysis probes into the dorsomedial mediobasal hypothalamus of mutant mice and their control littermates (Figure 4F). In agreement with the P-STAT3 distribution observed under physiological conditions (Supplementary Figure 7), basal leptin levels in this region, before any dilution effect of peripheral vehicle injection, were seen to be significantly lower in *LepR*^{TanKO} mice (0.8±0.5 pg/ml) than in *LepR*$^{loxP/loxP}$ littermates (26.5±7.5 pg/ml, t-test, p=0.0196). In addition, 20 min after an i.p. bolus injection of leptin, *LepR*$^{loxP/loxP}$ mice displayed a significant early peak in hypothalamic leptin levels before reaching an intermediate plateau and a second peak at 80 minutes, which were both absent in *LepR*^{TanKO} mice (Figure 4F); in

343 the latter mice, leptin levels merely showed a small and non-significant rise at 60 min but remained at
344 near-nadir levels otherwise (Figure 4F).

345 Similarly, mice in which EGFR expression in tanycytes was blunted by the AAV1/2-mediated
346 expression of *Egfr* silencing RNAs in these cells (Supplementary Figure 4B, Figure 4G) phenocopied
347 certain aspects of *LepR*^{TanKO} mice, notably the concomitant decrease in lean mass and increase in fat
348 mass with no modification of body weight 8 weeks after infection, when compared with mice infected
349 with a control virus expressing GFP (Figure 4H, 4I and 4J). Like *LepR*^{TanKO} mice, animals with EGFR
350 silencing in tanycytes also showed a hampered ability to respond to an i.p. injection of leptin by
351 decreasing food intake (Figure 4K).

352 Altogether, these results strongly support the view that tanycytic LepR-EGFR signaling is required
353 for blood-borne leptin to be transported into the hypothalamus and exert its anorexigenic effect, and
354 reveals an unpreceded role for tanycytic leptin transport in the control of body composition.
355
356
357 **Mice lacking LepR in tanycytes show hyperlipidemia and lipid accumulation in white**
358 **adipocytes as well as in the liver**

359 Given the increase in RER in *LepR*^{TanKO} mice (Figure 3M), indicative of the increased consumption
360 of carbohydrates over lipids to meet energy requirements [40], we next examined how lipid metabolism
361 was altered in mice in which leptin transport into the hypothalamus was defective. The changes in
362 RER and food-intake-independent body weight gain in *LepR*^{TanKO} mice appeared to be due to
363 decreased fatty acid oxidation (Figure 5A), which was associated with an increase in both visceral fat
364 mass (Figure 3I) and leptinemia (Figure 3O) and elevated circulating levels of cholesterol and
365 triglycerides (Figure 5B), but not of non-esterified free fatty acids (NEFAS) (Figure 5C). These data,
366 together with an increase in the size of white adipocytes (Figure 5D), suggest that *LepR*^{TanKO} mice
367 show hyperlipidemia and lipid accumulation in white adipocytes.

368 In agreement with the increased uptake of free fatty acids into white adipose tissue in response to
369 central leptin deficiency [13], *LepR*^{TanKO} mice showed a marked increase in protein levels of lipoprotein
370 lipase (LPL), an enzyme that promotes the uptake of circulating triglycerides, and acetyl-CoA
371 carboxylase (Acc) and fatty acid synthase (FAS), enzymes crucial for *de novo* lipogenesis, in
372 ependymal fat (Figure 5E and 5F). Of note, the ratio of phospho-Acc to total Acc was decreased in

373 *LepR*^{TanKO} mice (Figure 5E and 5F), which suggests, in agreement with previously published data [13],
374 that hypothalamic leptin regulates ACC in white adipose tissue. We next examined the expression of
375 the key lipolytic enzyme hormone-sensitive lipase (HSL), the activity of which is also known to be
376 regulated by central leptin signaling [13], and found that the levels of phosphorylation-activated HSL
377 were lower in *LepR*^{TanKO} mice than in control littermates (Figure 5E and 5F). Overall, these results
378 indicate that the lack of LepR in tanycytes favors the accumulation of lipids by promoting lipogenesis
379 and lipid uptake while inhibiting lipolysis in white adipose tissue. Importantly, these effects were
380 independent of feeding since they occurred in both *LepR*^{TanKO} mice fed *ad libitum* and those pair-fed
381 with the control group.
382 Increased accumulation of lipids was also noted in the liver of *LepR*^{TanKO} mice using oil red staining
383 (Figure 5G). Accordingly, liver triglyceride content was seen to be increased in these mice even in the
384 pair-fed condition (Figure 5H), whereas circulating triglyceride levels were comparable to those in
385 *LepR*$^{loxP/loxP}$ controls (Figure 5B). Given the absence of any marked change in the expression of
386 enzymes involved in lipid metabolism (Figure 5I and 5J), the increase in lipid accumulation in the liver
387 of *LepR*^{TanKO} mice is likely not due to local *de novo* synthesis but indirectly to the increased weight and
388 hyperlipidemia of these mice.
389
390 **Mice lacking LepR in tanycytes sequentially develop impaired glucose tolerance and defective**
391 **insulin-secretory capacity**
392 Leptin has long been known to influence glucose homeostasis independent of its effect on body
393 weight regulation [41,42]. These effects appear to be mediated by leptin action on LepR-expressing
394 neurons in the ARH, since the local reintroduction of LepR expression in otherwise LepR-knockout
395 animals normalizes insulinemia in these animals [11]. In light of the altered gene expression in ARH
396 neurons observed in our mice, we therefore next investigated the effect of LepR deletion in tanycytes
397 in glucose metabolism. Four weeks after LepR deletion, mice did not appear to have any problem in
398 managing exogenous injections of glucose (Figure 6A). However, monitoring glucose-stimulated
399 insulin release in *LepR*^{TanKO} mice at 4 weeks intriguingly showed that, despite normal glucose
400 tolerance at this early time point (Figure 6A), these mice were secreting more insulin than control
401 *LepR*$^{loxP/loxP}$ or *LepR*^{TanHet} mice both before (12h fasting insulin: *LepR*^{TanKO}, 0.81 $\pm$ 0.12 μg/μl vs.
402 *LepR*$^{loxP/loxP}$, 0.48 $\pm$ 0.06 μg/μl and *LepR*^{TanHet}, 0.46 $\pm$ 0.03 μg/μl, $p = 0.03$ and $p = 0.04$, respectively,

one way ANOVA and Tukey's multiple comparison test) and after glucose injection (Figure 6B), despite an apparently normal response to insulin (Figure 6C), suggestive of a pancreatic β-cell function deficiency. This elevated release of insulin by β-cells even under basal conditions phenocopies mice lacking LepR in POMC neurons [43], concordant with an inability of ARH neurons to appropriately perceive circulating leptin levels as suggested by decreased STAT3 activation after overnight feeding (Supplementary Figure 7) or upon exogenous leptin treatment (Figure 4A, 4C), as well as the downregulation of *Socs3* in the ARH of *LepR*^{TanKO} mutants (Figure 4D).

By 12 weeks after LepR deletion, however, *LepR*^{TanKO} mice developed impaired tolerance to exogenous glucose (Figure 6D), while their basal insulin levels were similar to those in *LepR*$^{loxP/loxP}$ mice. This deficient glucose homeostasis was also correlated with a significantly lower increase in glucose-stimulated insulin levels in *LepR*^{TanKO} mice, suggesting some degree of pancreatic dysfunction in these mice (Figure 6E). Insulin sensitivity and HOMA-IR were similar in the two genotypes (Figure 6F and 6G). To investigate possible alterations in pancreatic function in mice lacking LepR in tanycytes, we investigated glucose-stimulated insulin secretion (GSIS) in isolated pancreatic islets from *LepR*^{TanKO} and *LepR*$^{loxP/loxP}$ littermates. Although *LepR* deletion in tanycytes did not affect the total insulin content of islets (Figure 6H), insulin secretion from isolated islets was severely hampered under high glucose conditions in 12-week *LepR*^{TanKO} mice when compared to *LepR*$^{loxP/loxP}$ controls (Figure 6I). Gene expression analysis in islets from 12-week *LepR*^{TanKO} mice compared to controls revealed the increased expression of genes involved in glucose sensing (*Glut2, Gck*) and insulin maturation (*Pcsk1*) but decreased expression of key β–cell identity genes such as *Pdx1* (p=0.065) and *MafA* (Figure 6J). *LepR*^{TanKO} islets also exhibited an increase in the expression of markers of the endoplasmic reticulum (ER) unfolded protein response (UPR^{er}) pathway, including *Atf4 (*p=0.016*)*, *Xpb1t* and *Chop* (Figure 6K), thought to be associated with impaired β–cell function and T2D development [44]. The number of α (glucagon-positive) and β (insulin-positive) cells per islet was similar in the pancreas of the two genotypes (Figure 6L, 6M, 6N). Altogether, these data suggest that the loss of *LepR* function in tanycytes impairs glucose homeostasis and insulin secretion through the transcriptional control of key pancreatic β–cell and UPR^{er} markers, preceded by the development of mild insulin resistance, and that the whole sequence of events unfolds within 3 months of altering the tanycytic shuttling of leptin into the hypothalamus.

To determine whether the restoration of hypothalamic access to leptin could rescue β-cell function in 12-week *LepR*^{TanKO} mice, we deprived animals of food 3h before stereotaxically injecting them with 2 μg of leptin i.c.v., shortly before lights-off. At lights-on, i.e. 12h after leptin injection in food-deprived animals, a glucose tolerance test was performed by injecting glucose i.p. Pre-treatment with acute i.c.v. leptin significantly rescued the impaired glucose management in *LepR*^{TanKO} mice, without further depressing glycemia in *LepR*$^{loxP/loxP}$ littermates (Figure 6O). In addition, while glucose-stimulated insulin secretion at 15 min was lower in mice lacking tanycytic LepR than in *LepR*$^{loxP/loxP}$ littermates in the absence of leptin pre-treatment, as shown above (Figure 6E), the central administration of leptin significantly increased insulin secretion 15 min after glucose injection in both mutant and control mice, compensating for the defective tanycytic function (Figure 6P). These results demonstrate that the action of tanycyte-transported leptin in the hypothalamus is vital for the acute control of β-cell function directly by the brain, likely through the intermediary of leptin-sensing ARH neurons connected to the pancreas via the autonomic nervous system [43], and raise the intriguing possibility that defects in the tanycytic leptin shuttle may also play a critical central role in the pathophysiology of diabetes.

Impaired access of leptin to the hypothalamus could mediate central effects on glucose and lipid metabolism through altered sympathetic tone

The central effects of leptin on glucose homeostasis appear to involve the melanocortin system [43], which we have shown above to be altered in *LepR*^{TanKO} mice, and which impinges upon the sympathetic nervous system [45,46]. In addition, the sympathetic nervous system is also known to mediate the central effects of leptin on white adipose tissue lipid metabolism [13]. We therefore next assessed circulating noradrenaline levels in *LepR*^{TanKO} mice, with their defective tanycytic shuttling of leptin into the hypothalamus (Figure 4E and 4F), and found that the levels of noradrenaline were reduced, suggesting an overt decrease in sympathetic tone when compared to control *LepR*$^{loxP/loxP}$ littermates (Figure 7A). Interestingly, the pancreatic islets of *LepR*^{TanKO} animals express more α2A adrenergic receptors compared to their littermates without affecting the expression of β2 adrenergic receptors (Figure 7B). α2A adrenergic receptors are known for their inhibitory action on insulin secretion by the pancreas [47,48]. To further probe the sympathetic nervous system in *LepR*^{TanKO} mice, we subjected them to a 2h exposure to cold (4°C) and measured changes in rectal temperature as well as noradrenaline levels. In cold conditions, *LepR*^{TanKO} mice experienced a drop in core

462 temperature (Figure 7C), a phenomenon associated with defective cold-induced noradrenaline
463 secretion (Figure 7D). Together, these results suggest a possible mechanistic pathway whereby
464 decreased leptin access to hypothalamic neurons controlling bodily homeostasis alters overall
465 sympathetic tone, which in turn affects peripheral glucose and lipid metabolism. Because previous
466 studies have shown that brain-pancreas and brain-adipose tissue connections involve leptin signaling
467 through the melanocortin system [43,49] and because *LepR*^{TanKO} mice show altered levels of *Agrp*
468 transcripts (Figure 4D), it is tempting to speculate that the main hypothalamic neuronal population
469 affected by the defective shuttling of circulating leptin into the brain is that of AgRP-expressing ARH
470 neurons, which mediate melanocortin signaling.
471
472 **Knocking out LepR in tanycytes blunts the leptin-mediated neuroendocrine response to fasting**
473 Given our previous demonstration that tanycytes play a role in the adaptive response to fasting [22], and
474 because leptin has long been known to play important physiological roles during starvation [50], we next
475 tested the ability of peripheral leptin treatment (1mg/kg/12h) to attenuate the adaptive neuroendocrine
476 response to 24h fasting in *LepR*^{TanKO} mice. While leptin repletion after this period of starvation had no
477 effect on blood glucose, it caused a reduction in food intake over the first 4h and 12h of refeeding and
478 a consequent reduction in weight gain after 24h in *LepR*$^{loxP/loxP}$ mice, but not in *LepR*^{TanKO} littermates
479 (Figure 7E). Interestingly, while 24h fasting dramatically increased corticosterone levels in *LepR*$^{loxP/loxP}$
480 mice, a phenomenon normalized by leptin replacement therapy, it did not cause any change in
481 corticosterone levels in *LepR*^{TanKO} mice (Figure 7E).
482 Overall, our results strongly suggest that in the absence of the tanycytic leptin shuttle, the brain loses
483 its ability to properly respond to physiological challenges and thus to restore bodily homeostasis.
484
485
486 **DISCUSSION**
487
488 Leptin, a hormone secreted by adipocytes in the periphery, plays a fundamental role in the regulation
489 of energy homeostasis by controlling food intake and energy expenditure [4-9]. To achieve its central
490 effects, leptin needs to cross the blood-brain barrier and gain access to specific leptin-sensitive
491 neurons in the hypothalamus and elsewhere, a process mediated by tanycytes [23]. Our results
492 convincingly show that, in contrast to recent studies that question the expression of the leptin receptor
493 LepR in tanycytes [25], LepR is not only expressed but is functionally active in hypothalamic median

494 eminence tanycytes, and transports leptin into the hypothalamus in a leptin- and EGF-dependent
495 manner by forming a complex with EGFR.
496 Possible explanations for the assumption that LepR is not expressed in tanycytes could be the fact
497 that, like astrocytes, these specialized hypothalamic glia do not express the cre-dependent reporter
498 genes commonly used in *LepR*::*Cre* animal models [24] or that most of the alternative detection
499 techniques used so far are not sensitive enough [25]. In addition, in the inducible Cre-driver mouse lines
500 used by others [25], the accessibility of the *LepR* gene in tanycytes may be impaired by the use of
501 tamoxifen, which is known to alter chromatin architecture [51], interfere with estrogen receptor activity
502 and impact metabolism on its own [52]. These technical problems were overcome in the current study
503 with an array of methods to detect not only the presence of LepR protein in ME tanycytes but also its
504 function. In addition, we demonstrate that LepR signaling in tanycytes plays a critical role in the
505 transcytotic mechanism by which they shuttle blood-borne leptin into the hypothalamus, and show that
506 the leptin-mediated activation of LepR causes the early activation of EGFR, which we had previously
507 and serendipitously shown to be able to rescue diet-induced obese animals from central resistance to
508 peripheral leptin [23]. This leptin-LepR-dependent activation of EGFR in tanycytes, which our PLA
509 experiments suggest occurs in tanycytic distal processes that contact the fenestrated endothelium of
510 pituitary portal capillaries *in vivo*, is required for the release of internalized leptin from early
511 endosomes by triggering the downstream ERK signaling pathway. Furthermore, while LepR and
512 EGFR appear to form a complex capable of binding both leptin and EGF, the activation of EGFR by
513 EGF potentiates the effects of leptin on ERK activation while it appears to leave P-STAT3 activation
514 unaffected. The kinetics of EGFR and ERK activation by leptin in primary tanycytes, with the leptin-
515 induced phosphorylation of EGFR occurring at very early time points, within 2 minutes as seen by
516 PamGene technology, and ERK phosphorylation occurring at 15 min, is reminiscent of that reported in
517 gastric cancer cells [53]. Although we detected EGF in the circulation in our animals, this EGFR
518 activation in tanycytes could also involve *trans*-activation processes, similar to those observed in
519 cancer cells [53] and also known to occur in tanycytes [54,55].
520 Leptin signaling in the brain also exerts specific and complementary peripheral effects on adipose
521 tissue through the regulation of nutrient partitioning by decreasing the expression of key de novo
522 lipogenic enzymes and stimulating the levels of phosphorylated HSL, essential for the activation of
523 lipolysis [7,13]. Interestingly, in addition to its mild consequences on body weight, we show that deleting

524 tanycytic LepR expression in the median eminence of adult mice increases food intake, modifies
525 nutrient partitioning to favor the disproportionate use of carbohydrates, thus favoring lipid
526 accumulation, dramatically alters body composition by promoting an increase in fat mass to the
527 detriment of lean mass, and also impairs the ability of the brain to control glucose homeostasis in
528 association with a marked impairment in pancreatic β-cell function and altered sympathetic tone.
529 The capacity of leptin to regulate these diverse metabolic parameters resides in LepR-expressing
530 neurons in the ARH, namely proopiomelanocortin (POMC) and agouti–related peptide (AgRP)
531 expressing neurons, which are known to be involved in the control of adipose tissue lipogenesis [13] and
532 glucose homeostasis [11], in response to this adiposity signal. For instance, the deletion of LepR in
533 either POMC or AgRP neurons leads to moderate obesity, while the knock-out of LepR in both AgRP
534 and POMC neurons combined has clear cumulative effects on adiposity despite a comparable effect
535 on food intake [56,57]. The fact that our mice mimic this metabolic phenotype suggests that the depletion
536 of LepR in tanycytes precludes the access of leptin to POMC and AgRP neurons and its subsequent
537 actions in these neuronal populations. This hypothesis is supported by the fact that the removal of
538 LepR form tanycytes severely hampers the ability of both endogenous and exogenous leptin to reach
539 the mediobasal hypothalamus and activate leptin-sensitive neurons in the dmARH, and upregulates
540 transcripts for *Agrp*, a melanocortin receptor antagonist, while downregulating the expression of
541 *Socs3*, a known leptin-responsive gene [36], in the ARH. Interestingly, the melanocortin system is
542 involved not only in glucose homeostasis [11,43,58] but also in the sympathetic nervous system-mediated
543 regulation of lipid metabolism in white adipose tissue [13,49], and both nadir and cold-induced circulating
544 noradrenaline levels are reduced in mice lacking tanycytic LepR. In light of these findings, we propose
545 that deficient leptin-regulated activity in POMC and AgRP neurons of the dmARH alters their capacity
546 to use the melanocortin signaling pathway [59,60] to communicate with neurons of the autonomous
547 nervous system in the brainstem and the spinal cord [45,61], and thus their control of peripheral target
548 tissues [7,62]. In keeping with the hypothesis above, we found that the decrease in insulin secretion by
549 pancreatic β-cells in mice lacking LepR in tanycytes was associated with a significant increase in their
550 expression of α2A adrenergic receptors. This is also in agreement with previous studies showing that
551 the activation of these receptors is associated with a decrease in both glucose tolerance and insulin
552 exocytosis by β islets [47]. In addition, in humans, a polymorphism leading to the overexpression of the
553 α2A adrenergic receptor ADRA2A is associated with an increased risk of developing T2D [48]. Our

554 results suggest that the removal of leptin receptor expression in tanycytes may lead to a decrease in
555 insulin secretion that can be explained by an overexpression of adrenergic receptors α2A. Overall, our
556 results fill the gaps in our understanding of the mechanism of leptin action: i) blood-borne leptin
557 reaches dmARH neurons through a singular route involving transcytotic transport by median eminence
558 tanycytes, which depends on the activation of a LepR:EGFR complex and ERK signaling, ii) leptin
559 then stimulates the dmARH neurons controlling the melanocortin system and sympathetic outflow, and
560 iii) this diminishes lipid storage in adipose tissue and controls glucose homeostasis by shaping the
561 function and plasticity of pancreatic islet cells through their expression of α2A adrenergic receptors..
562 Conversely, alterations in tanycytic leptin transport manifest as decreased sympathetic tone,
563 increased visceral adiposity, hepatic steatosis and glucose intolerance with pancreatic dysfunction.
564 Interestingly, regardless of whether LepR or EGFR signaling in tanycytes is defective in our mouse
565 models, the fat mass gain observed occurs concomitantly with an intriguing loss of lean tissue,
566 resulting in overall weight gain remaining limited. This phenomenon, where obesity is associated with
567 sarcopenia (sarcobesity), is reminiscent of that often seen during aging [63,64] and may promote the
568 progression of related conditions such as diabetes and frailty [65]. A recent study has shown that in
569 mouse models of hyperglycemia and T2D due to defective β cell function, inter-tissue crosstalk
570 involving the liver and amino acid catabolism leads to skeletal muscle atrophy [66]. Further studies are
571 required to explore this pathway in mice in which LepR:EGFR signaling complex is defective in
572 tanycytes, to determine how alterations of the tanycytic leptin shuttle impact aging.
573 Longitudinal human studies show that T2D develops in subjects exhibiting insulin hypersecretion in
574 normoglycemic and prediabetic phases in order to keep glycemia near normal, in a context of chronic
575 nutrient surfeit and obesity-associated insulin resistance, until they reach a threshold at which this
576 compensatory β cell response becomes unsustainable [67]. Compensating for insulin resistance by
577 increasing insulin secretion usually requires both enhanced β cell function and expansion of the β cell
578 mass, the latter being stimulated by the increased nutrient supply, including glucose and free fatty
579 acids [68]. However, diabetes is a heterogeneous disease [69], and an alternative pattern characterized by
580 the alteration of insulin secretion due to a β cell functional deficit could predominate in some ethnic
581 groups. This phenotypic variability can be seen in a Japanese study in which the proportion of patients
582 progressing to the onset of T2D was 50% in patients with a dysfunction of isolated β cells, as
583 compared to 14% for patients with insulin resistance [70]. Intriguingly, an epidemiological study of

Korean patients with T2D showed that they developed impaired insulin secretion and insulin resistance 10 years before the onset of diabetes, and impaired β cell compensation with an abrupt decrease in insulin secretion during the last 2 years before onset [3], underscoring the central role of β cell dysfunction in the pathogenesis of T2D in Asian populations. The existence of two patterns of disease progression can also be seen from the fact that East Asian T2D patients have a much lower BMI than European patients but more intra-abdominal fat for similar BMI values [2]. In our current model, the attenuation of tanycytic leptin transport leads to an initial increase of insulin secretion despite the absence of insulin resistance. Twelve weeks after selectively deleting LepR in median eminence tanycytes, *LepR*^{TanKO} mice develop impaired insulin secretion in response to glucose, against a backdrop of increased visceral fat but normal insulin sensitivity. This alteration of glucose-stimulated insulin secretion, which likely underlies the alteration of glucose homeostasis, can be seen at the level of isolated pancreatic islets despite the lack of any apparent change in their size or organization, suggesting a modification of β cell functional integrity instead, mimicking the principal human phenotype described above. Despite this deficiency in β-cell function, the reactivation of central control by infusing leptin into the cerebral ventricles 12 weeks after the tanycytic leptin shuttle was inactivated by knocking out LepR restored the ability of these mice to manage exogenous glucose, by restoring insulin secretion induced by CSF-borne leptin.

To summarize, the study of our *LepR*^{TanKO} mouse model appears to have unmasked two important aspects of leptin action: i) the molecular and cellular mechanisms that regulate the physiological access of leptin to leptin-responsive neurons in the brain, i.e. the LepR-EGFR-ERK-mediated transcytotic transport of blood-borne leptin into the hypothalamus by tanycytes, and ii) the link between deficient leptin transport by tanycytes and the pathophysiology of pancreatic β-cell failure and lipid dysmetabolism in the context of moderate overweight and sarcobesity. Together, these findings shed light on the central control of peripheral lipid and glucose homeostasis by leptin, and create new therapeutic avenues for metabolic disorders.

METHODS

Animals

All C57Bl/6J mice were housed under specific pathogen-free conditions in a temperature-controlled room (21-22°C) with a 12h light/dark cycle and *ad libitum* access to food and water. *tdTomato*$^{loxP\text{-}STOP\text{-}}$

^{loxP} (IMSR Cat# JAX:007914, RRID:IMSR_JAX:007914) and GCamP3$^{loxp\text{-}STOP\text{-}loxP}$ (IMSR Cat# JAX:025406, RRID:IMSR_JAX:025406) reporter mice and *LepR*$^{loxP/loxP}$ mice (IMSR Cat# JAX:008327, RRID:IMSR_JAX:008327) [71] were purchased from the Jackson Laboratories (Bar Harbor, ME). *Trmp5*::*Cre* mice have been engineered by Dr. Ulrich Boehm (University of Saarland, Homburg, Germany) and published elsewhere [29]. Animal studies were approved by The Institutional Ethics Committees for the Care and Use of Experimental Animals of the University of Lille; all experiments were performed in accordance with the guidelines for animal use specified by the European Union Council Directive of September 22, 2010 (2010/63/EU).

TAT-Cre, pAAV-Dio2-iCre-2A-GFP and AAV(1+2)-GFP-U6-m-EGFR-shRNA delivery

A TAT-Cre fusion protein and the AAV 1/2 *Dio2*::*Cre* virus (0,5x1010 genomic particles per µl) were produced as detailed previously [31,72]. AAV(1+2)-GFP-U6-m-EGFR-shRNA was produced by Vector Biolabs (shAAV-258137). All products were stereotaxically infused into the third ventricle (2uL over 7 min at 1,27 mg/ml; anteroposterior, -1.7 mm; midline, 0 mm; dorsoventral, -5.6 mm), the lateral ventricle (Anteroposterior, -0.3 mm; midline, +/- 1 mm; dorsoventral, -3 mm) or the forth ventricle (Anteroposterior, -6 mm; midline, 0 mm; dorsoventral, -4 mm) of 24h fasting isoflurane-anesthetized floxed mice 1 week before experiments for the TAT-Cre one and 3 weeks before experiments for the virus one.

Evaluation of TAT-Cre recombination efficiency

Four weeks after lateral ventricle or 3rd ventricle TAT-Cre infusion in *TdTomato* mice, animals were anesthetized with ketamine (8mg/kg body weight) + xylazine (3mg/kg body weight) before being perfused with Saline (0,9% NaCl) and 4% paraformaldehyde. Brains were collected before being cryoprotected in 20% sucrose solution overnight, embedded in Tissue Tek (Sakura®) and frozen freshly. 16 µm-thick coronal sections were cut and processed for immunofluorescence using chicken anti-Vimentin (1:2000; Millipore Cat# AB5733, RRID:AB_11212377) primary antibodies and Alexa647-conjugated anti-chicken antibody (1/1000; Thermo Fisher Scientific Cat# A-21449, RRID:AB_2535866). Images were acquired using an Axio Imager Z2 Apotome microscope (AxioCam MRm camera, Zeiss). 8 median eminence representative slides per animal were then coded to conceal treatment groups and the tanycytes (Vimentin positive cells) were divided into three groups

depending their projections (median eminence and arcuate nucleus, ventromedial hypothalamus, dorsomedial hypothalamus). Number of DAPI+/Tomato+/Vimentin+ cells was reported on DAPI+/Vimentin+ cells bording the 3rd ventricle. The ratio was compared between different groups. To compare 3rd and 4th ventricle TAT-Cre infusion, the number of FACS -sorted Tomato positive cells was compared in ME and 4th ventricle microdissected samples, 1 week after TAT-cre infusion.

Fluorescence-Activated Cell Sorting and Real-Time PCR Analyses

Isolation of hypothalamic tanycytes using Fluorescence Activated Cell Sorting

Median eminence from TAT-Cre injected *tdTomato*$^{loxP/+}$ and *LepR*$^{oxP/loxP}$; *tdTomato*$^{loxP/+}$ mice were microdissected, and enzymatically dissociated using Papain Dissociation System (Worthhington, Lakewood, NJ) to obtain single-cell suspensions. FACS was performed using an ARIA SORP cell sorter cytometer device (BD Bioscience, Inc). The sort decision was based on measurements of tdTomato fluorescence (excitation 561nm; detection: bandpass 675+/-20nm) by comparing cell suspensions from tdTomato positive and wild-type animals, as indicated in Figure 3A. For each animal, 4000 cells tdTomato positive and negative cells and negative cells were sorted directly into 10µL extraction buffer: 0,1% Triton® X-100 (Sigma-Aldrich) and 0,4 U/µl RNaseOUT™ (ThermoFisher).

Quantitative RT-PCR analyses

For gene expression analyses, mRNAs obtained from microdissected hypothalamic explants or FACS-sorted tanycytes were reverse transcribed using SuperScript® III Reverse Transcriptase (Life Technologies) and a linear preamplification step was performed for the sorted cells only using the TaqMan® PreAmp Master Mix Kit protocol (P/N 4366128, Applied Biosystems). Real-time PCR was carried out on Applied Biosystems 7900HT Fast Real-Time PCR System using exon-boundary-specific TaqMan® Gene Expression Assays (Applied Biosystems): DARPP32 (Ppp1r1b_Mm00454892_m1); LEPR (Variant 1, long form) (LepR_Mm1265583_m1); LEPR (Variant 3, short form) (LepR_Mm01262070_m1), NPY (NPY-Mm03048253_m1), MECA32 (Plvap-Mm00453379_m1), POMC (POMC-Mm00435874_m1), AgRP (AgRP-Mm00475829_g1), CART (CARTPT-Mm04210469_m1), Socs3 (Socs3-Mm00545913_s1), Ptp1b (Ptp1b-Mm00448427_m1) DIO2 (Dio2-Mm00515664_m1), FGF10 (Fgf10-Mm00433275_m1), GPR50 (Gpr50-

Mm00439147_m1), SLCO1C1 (Slco1c1-Mm00451845_m1). Control housekeeping genes: r18S (18S-Hs99999901_s1); ACTB (Actb-Mm00607939_s1). Gene expression data were analyzed using SDS 2.4.1 and Data Assist 3.0.1 software (Applied Biosystem).

Physiological measurements

Body Composition

Body composition was measured weekly in several cohorts of mice using Minispec LF Series (Bruker Corporation, Massachusetts). Data on fat mass, lean mass and free liquid mass were collected and expressed as % of body weight.

Analysis of basal metabolism

Mice were analyzed for total energy expenditure, oxygen consumption and carbon dioxide production, food intake and ambulatory movements (total beam breaks/h) using calorimetric cages (TSE Systems GmbH, Germany) and standard procedures. Mice were individually housed and acclimatized to the cages for 48h before experimental measurements. During the pair-fed test, paired-fed animals had the mean weight of food that the control group ate during the previous 24 hours (see paragraph below). RER and energy expenditure (EE) were calculated as previously reported by us [73,74], and fatty acid oxidation was calculated using the formula reported by Bruss and colleagues [75]:

$$\text{FA oxidation (kcal/h)} = EE \times (1 - RER/0.3)$$

Pair-feeding experiments

Pair-feeding experiments were performed as documented previously [76,77]. Briefly, we assessed food intake under normal conditions in both $LepR^{loxP/loxP}$ and $LepR^{TanKO}$ mice for at least one week without performing any type of experiment and avoiding any stress. Then, we pair-fed $LepR^{TanKO}$ mice with the group showing lower food intake, i.e., $LepR^{loxP/loxP}$ mice. To avoid long periods of fasting that could alter the results obtained from the pair-fed group, pair-fed $LepR^{TanKO}$ mice mice received 2/3 of their daily amount of food just before the dark phase (the active period when mice consume the highest amounts of food) and 1/3 at lights-on (the period when mice are inactive and consume low amounts of food).

Glucose Tolerance Test and Insulin dosage

Mice were fasted overnight before the experiment (12 hours). Blood sample for insulin dosage was taken before, 15 and 30 min after glucose administration with glass capillary at the tail. Samples were kept on ice during the experiments before being centrifuged (4°C, 600 rpm, 15 min) to collect serum and frozen at -80°C until insulin ELISA (Mercodia). Basal blood glucose level was measured before glucose i.p administration (1,5 mg glucose/g of body weight), 15, 30, 45, 60, 120 and 150 min after glucose administration using glucometer (OneTouch® Verio meter). One cohort of animals was injected i.c.v with recombinant murine leptin (2µg/animal; Harbor-UCLA Medical Center, California) 3 hours before lights-off, mice subjected to fasting overnight (12 hours) and glucose tolerance test as well as insulin dosage performed the next day.

Insulin Tolerance Test

Mice were fasted 6 hours before the experiment. Basal blood glucose level was measured before insulin i.p administration (0,75UI/kg of body weight), 15, 30, 45, 60, 120 and 150 min after glucose administration using glucometer (OneTouch® Verio meter)

In vivo leptin sensitivity test

Mice were first separated one per cage and fasted during 3 hours in the afternoon. Then they are divided into two groups which received i.p or i.c.v injections of recombinant murine leptin (3mg/kg; Harbor-UCLA Medical Center, California) or vehicle (PBS pH 8.0) 3 hours before being reefed. Body weight and food intake were measured before, 12h and 24h after treatment period.

Assessment of the role of leptin in the corticosterone response to 24h fasting

Two weeks before fasting, at lights-on (8 am), glycemia was measured and blood was drawn from the animal's cheek [78] to assess serum corticosterone levels in the fed condition. Then, mice were put in individual cages and subjected to fasting for 24 hours. Half the fasting mice received leptin (1mg/kg; Harbor-UCLA Medical Center, California) while the other half received saline i.p. injections every 12 hours (8 am and 8 pm). After 24h of fasting, blood samples were taken from each animal's cheek before refeeding. Food intake was then measured at 4, 12 and 24 hours after refeeding.

Corticosterone levels were quantified by ELISA (55-CORMS-E01; American Laboratory Products Company) according to manufacturer's instructions.

Cold-exposure test: core temperature and noradrenaline measurements

Rectal temperature was measured in mice before collecting blood samples from the cheek. One hour later, mice were exposed to cold (4°C) for 2 hours, then rectal temperature was taken and blood collected. Delta temperature (difference between before and after cold exposure) was calculated and fed and fasting noradrenaline serum concentrations were quantified by ELISA (see paragraph below).

Microdialysis *in vivo*

Nine *LepR*$^{loxP/loxP}$;*tdTomato*$^{loxP\text{-}STOP\text{-}loxP}$ mice were injected in the lateral ventricle with the AAV(1/2) *Dio2::Cre* virus (n=4) or vehicle (n=5). In brief, 25-35g mice were deeply anesthetized with isoflurane (3% in 1 L/min air flow) in an induction chamber, placed in a stereotaxic apparatus equipped with a mask to maintain anesthesia during all the experiment (isoflurane between 1 to 1.5% in 1 L/min air flow). Core body temperature was maintained at 37◦C with an electrical blanket controlled by a thermostat. A microdialysis cannula (CMA8 High Cut-off, 100 kDa, 1 mm membrane length; CMA microdialysis AB, Sweden) was implanted over the mediobasal hypothalamus using the stereotaxic coordinates (relative to bregma antero-posterior: -1.3, lateral: −0.3, ventral from brain: −6.1 mm). The microdialysis probe was then perfused with sterile artificial cerebrospinal fluid (CMA Perfusion Fluid CNS. NaCl 147 mmol/L, KCl 2.7mmol/L, CaCl2, 1.2 mmol/L and MgCl2 0.85 mmol/L; CMA, Stockholm, Sweden) at a rate of 2 µL/min using a microinjection pump (CMA 402; CMA, Stockholm, Sweden). Following a stabilization period of 45 min, one dialysate of 20 min was collected as basal. A vehicle injection (i.p, PBS pH 8.0) was administered to the mice and two dialysates of 20 min were recovered. Finally, at 60 min, a leptin solution was administered to the mice (i.p, 3mg/Kg in PBS pH 8.0, Harbor-UCLA Medical Center, California) and 5 dialysates of 20 min each were recovered. Brain dialysates were placed in a fraction collector (CMA/820) during the experiment and immediately stored at −80°C until analysis. At the end of the experiment, mice were euthanized by decapitation and brains stored immediately in fresh paraformaldehyde 4%. Vibratome brain sections of 80 µm were counterstained with DAPI to verify probe location. Only mice in which the probe was positioned between antero-posterior: -1.2 and -2.3 were included in the analysis.

Leptin, EGF and noradrenaline ELISA assays

Basal leptin concentration in the serum of *LepR*$^{loxP/loxP}$ and *LepR*^{TanKO} mice and leptin content in microdialysates from the brain were measured using ELISA (Leptin mice MOB00; R&D systems) according to the manufacturer's protocol. EGF concentration in blood serum from C57Bl/6J mice fed normal chow or 8 weeks of high-fat diet (#D12492; Research Diets), *LepR*$^{loxP/loxP}$ and *LepR*^{TanKO} mice were quantified by ELISA according to the manufacturer's instructions using a mouse EGF ELISA kit (EMEGF ; ThermoFisher). Basal noradrenaline concentrations in the serum of *LepR*$^{loxP/loxP}$ and *LepR*^{TanKO} mice were quantified using a noradrenaline ELISA kit (BA-E5200; Immusmol).

Brain and peripheral tissues analysis

Brain slice preparation and calcium imaging

Eight to 12 week-old male *GCaMP3*^{Trmp5} and *GCaMP3*^{Trmp5}; *LepR*^{Trmp5} mice were anesthetized with isoflurane, and after decapitation, the brain was rapidly removed and put in ice-cold oxygenated (O_2 95% / CO_2 5%) artificial cerebrospinal fluid (ACSF) containing the following (in mM): 120 NaCl, 3.2 KCl, 1 NaH_2PO_4, 26 $NaHCO_3$, 1 $MgCl_2$, 2 $CaCl_2$, 10 glucose (300 mOsm, pH 7.4). After removal of the cerebellum, the brain was glued and coronal hypothalamic slices 200 µm thick containing the median eminence and lateral walls of the third ventricle were cut using a vibratome (VT1200S; Leica) as previously described [79]. Before recording, slices were incubated at 35ºC for a recovery period of 1 h. After recovery, slices were placed in a submerged recording chamber (31ºC; Warner Instruments) and continuously perfused (2 ml/min) with oxygenated ACSF. Tanycytes were observed with a 40x water immersion objective in an upright Leica DM-LFSA microscope by using infrared differential interference contrast (IR-DIC). To detect GFP fluorescence, a blue illumination was provided via a 470 nm LED and an ORCA-Flash4.0 LT digital CMOS camera (Hamamatsu) was used to collect images. MetaMorph image acquisition software (Molecular Devices) was used to control the illumination and camera. Analysis of imaging data was performed off-line using MetaMorph (Molecular Devices) and Fiji software. Regions of interest (ROI) were drawn around individual tanycyte cell bodies from the infrared and/or the fluorescence images. Changes in fluorescence intensity of GCaMP3 were measured by plotting the intensity of ROI over time, after the intensity of a background ROI had been subtracted. Then, an initial baseline fluorescence signal was computed before drug application at

resting state (F0) and subsequent fluorescence values (F-F0=ΔF) were normalized to this (ΔF/F0). Drugs were applied via puffs from a patch pipette made of borosilicate glass (World Precision Instruments) and pulled on a P1000 puller (Sutter Instrument Co). The tip of the pipette was positioned 25 µm away from tanycyte cell bodies. Puffs were delivered in the opposite direction of the flow of the perfusion chamber at a pressure of 4 psi using a PV820 pneumatic PicoPump (World Precision Instruments). The concentration of Leptin and ATP (Sigma) in the patch pipette was 6 µM and 10 mM (both prepared in ACSF), respectively. To exclude mechanical responses of tanycytes to the puff, patch pipettes were also filled with ACSF alone.

Leptin receptor detection with the XPA antibody

Twelve week-old C57Bl/6J mice were anesthetized with ketamine (8mg/kg body weight) + xylazine (3mg/kg body weight) before being injected with the XPA antibody (2 nmol/animal, Xoma Laboratories) into the jugular vein. As soon as the injection ended, mice were perfused with saline (0,9% NaCl) and 4% paraformaldehyde. Brains were collected before being cryoprotected in 20% sucrose solution overnight, embedded in Tissue Tek (Sakura®) and fresh-frozen. 20 µm-thick coronal sections were cut and processed to reveal XPA using a 1 hour incubation at room temperature with Biotinylated Goat anti-human IgG (1:1000; Jackson ImmunoResearch Labs Cat# 109-065-003, RRID:AB_2337621). VECTASTAIN ® Elite ABC peroxidase kit (PK-6100, Vector Laboratories) used according to the manufacturer's instructions to amplify the signal. The XPA antibody was visualized with a TSA Biotin Tyramide kit (SAT70001EA, Perkin Elmer) associated with Streptavidin Alexa Fluor® 568 (1:600; Thermo Fisher Scientific Cat# S-11226, RRID:AB_2315774).

Proximity Ligation Assay

Brain sections were fixed in 4% paraformaldehyde for 15 min, permeabilized and saturated with Triton X100 (0.3%) and 5% Horse Serum/PBS solution for 1 h. Sections were incubated with primary antibodies XPA (Xoma Laboratories) and rabbit anti-EGFR (Sigma, Ab-1070) at 4 °C overnight. PLA was performed using a Duolink® In Situ Red Starter Kit Goat/Rabbit (Sigma-Aldrich) according to the manufacturer's protocol. To assess the specificity of the PLA signal, the whole process was performed with only one primary antibody.

RNAscope fluorescent in situ hybridization

FISH was performed on 2% paraformaldehyde perfused brain sections (*Egfr*) and frozen brain sections (*LepR*) of the median eminence of adult male mice using the RNAscope® Multiplex Fluorescent Kit v2 according to the manufacturer's protocol (Advanced Cell Diagnostics, Inc., Newark, CA, USA). Specific probes were used to detect *LepR* variant 1 (471171, NM_146146.2 , target region 3220 - 4109), *LepR* variant 3 (496901-C3 , NM_001122899.1 , target region 3291 - 4713), and *Egfr* (443551-C2 , NM_207655.2 , target region 58-2111) mRNAs. Hybridization with a probe against the Bacillus subtilis dihydrodipicolinate reductase (dapB) gene (320871) was used as a negative control. Following *Egfr* FISH,vimentin immunolabeling was carried out using a chicken anti-Vimentin antibody (1:500 Millipore Cat# AB1620, RRID:AB_90774), revealed with Goat anti-chicken 647 (1:500 ; Thermo Fisher Scientific Cat# A-21449, RRID:AB_2535). For FISH experiments and immunofluorescence labeling of Vimentin, the acquisition of images was performed using an inverted confocal microscope (LSM 710, Zeiss, Jena, Germany). Excitation wavelengths of 493/562 nm, 568/643 and 640/740 were selected to image Alexa 488- and Alexa 568-secondary antibodies and TSA plus Fluorescein, Cyanine 3 and Cyanine 5. UV laser (wavelength of 355 nm) was used to image Hoechst and DAPI. Z-stack images were acquired with a W Plan-APOCHROMAT 20x objective (NA 0.5, zoom 1.0). High magnification photomicrographs were acquired with a 63x objective (NA 1.4) using the Airyscan detector (Zeiss). Images to be used for figures were pseudocolored, adjusted for brightness and contrast and merged using Photoshop (Adobe Systems, San Jose, CA).

pSTAT3 immunohistochemistry and analysis

Adult mice were sacrificed by decapitation in the morning at lights on. Brains were collected before being embedded in Tissue Tek (Sakura®) and frozen freshly. 20 μm-thick coronal sections were cut, postfixed with a solution of 2% paraformaldehyde during one hour and processed for immunofluorescence as previously described (Bouret et al., 2012) using rabbit anti-pSTAT3 (Tyr705) (1:1000; Cell Signaling Technology Cat# 9131, RRID:AB_331586) primary antibodies and revealed with Goat anti-rabbit 647 (1/500; Molecular Probes Cat# A-21244, RRID:AB_141663). Immunofluorescence images were acquired using an Axio Imager.Z2 Apotome microscope (AxioCam

MRm camera, Zeiss). Slides were then coded to conceal treatment groups, and pSTAT3 immunoreactive (IR) cells counted in eight sections par animal.

Pancreatic Islet Studies

Pancreata were digested by type V collagenase (C9263; 1,5 mg/ml) for 11 min at 37°C as described previously (Annicotte et al., 2009, Rabhi et al., 2016). Briefly, after digestion and separation in a density gradient medium, islets were purified by handpicking under macroscope and cultured overnight in a 1640 RPMI (Gibco, 61870-010) media containing 1mM of FBS (Gibco, 10270-106) and Penicillin/streptomycin. For insulin secretion tests, approximately thirty islets were exposed to either 2,8 mM or 20 mM glucose in Krebs-Ringer bicarbonate HEPES buffer containing 0,5% fatty-acid-free BSA. Insulin released in the medium was measured 1 hour later using the Ultrasensitive Insulin ELISA kit (Mercodia). Data are expressed as a ratio of total insulin content..

RNA Extraction, Measurements and Profiling of pancreatic islets

Total RNA was extracted from islets using RNeasy Plus Micro Kit (Qiagen, Tokyo, Japan) according to the manufacturer's recommendations. mRNA expression was measured after reverse transcription by real-time qPCR with FastStart SYBR Green master mix (Roche) according to the manufacturer's recommendations and gene-specific oligonucleotides. Real-time qPCR results were normalized to endogenous cyclophilin reference mRNA levels. Results are expressed as the relative mRNA level of a specific gene expression using the formula $2^{-\Delta Ct}$. List of used primers are summarized in the table below.

Gene	Sense Primer	Antisense Primer
Cyclophiline	ATGGCACTGGCGGCAGGTCC	TTGCCATTCCTGGACCCAAA
Glut2	AACCGGGATGATTGGCATGT	GGCGAATTTATCCAGCAGCA
Gck	GCTCAGTGAACCCCGGTCAGC	TGTGCGCAGCTGCTCTGAGG
Kcnj11	CACAAGCTGGGTTGGGGGCTC	TGCCCCTCAGCTGGGTTCTGC
Glp-1r	GTTTCCTCACGGAAGCGCCA	AAGGAACCTGGGGGCCCATC
Ins1	GCCAAACAGCAAAGTCCAGG	GTTGAAACAATGACCTGCTTGC
Pcsk1	TGATGATCGTGTGACGTGGG	GGCAGAGCTGCAGTCATTCT
Pcsk2	AAAGATGGCGCTGCAACAAG	TTGCCCAGTGTTGAACAGGT
Pdx1	ATTGTGCGGTGACCTCGGGC	GATGCTGGAGGGCTGTGGCG
MafA	TCCGACTGAAACAGAAGCGG	CTCTGGAGCTGGCACTTCTC
Nkx2.2	GTGCAGGGAGTATTGGAGGC	GAAGGGCCAGAGGAGGAGA

Hnf1a	GGTGCGTGTCTACAACTGGT	ACCGTACACCGTGGACCTTA
Ucn3	TGATGCCCACCTACTTCCTG	CTGTGTTGAGGCAGCTGAAG
NeuroD1	CTTGGCCAAGAACTACATCTGG	GGAGTAGGGATGCACCGGGAA
ATF4	ATGGCCGGCTATGGATGAT	CGAAGTCAAACTCTTTCAGATCCATT
Xbp1t	GAGCAGCAAGTGGTGGATTT	CCGTGAGTTTTCTCCCGTAA
Xbp1s	GAGTCCGCAGCAGGTG	GTGTCAGAGTCCATGGGA
ChOP	CTGCCTTTCACCTTGGAGAC	CGTTTCCTGGGGATGAGATA
Ero1b	GGGCCAAGTCATTAAAGGAA	TTTATCGCACCCAACACAGT
PPP1R15a	GAGATTCCTCTAAAAGCTCGG	CAGGGACCTCGACGGCAGC
Pdia4	AGTCAAGGTGGTGGTGGGAAAG	TGGGAGCAAAATAGATGGTAGGG
Edem1	AAGTCTCAGGAGCTCAGAGTCATTAA	CGATCTGGCGCATGTAGATG

Immunofluorescence (IF) on pancreatic sections

IF was performed as described previously (Annicotte et al., 2009, Blanchett et al., 2011). Briefly, after antigen retrieval using citrate buffer (Sigma) 5 µm formalin fixed pancreatic sections were incubated with primary antibodies: Anti-Insulin (1:1000, Agilent Cat# A0564, RRID:AB_10013624), anti-Glucagon (1:1000, Sigma-Aldrich Cat# G2654, RRID:AB_259852). Immunofluorescence stainings were revealed using Goat Alexa 594-conjugated anti Guinea-Pig antibody (1:500, Molecular Probes Cat# A-11076, RRID:AB_141930) and Goat Alexa 488-conjugated anti-Mouse (1:500, Thermo Fisher Scientific Cat# A-11001, RRID:AB_2534069). Nuclei were stained with Hoescht. For morphometric analysis, images were processed by ImageJ software by an observer blinded to experimental groups.

Western Blot analysis on liver and WAT

Tissues were homogenized using a TissueLyser II (Qiagen, Tokyo, Japan) in cold RIPA buffer (containing 200 mMTris/HCl (pH 7.4), 130 mM NaCl,10%(v/v) glycerol, 0.1%(v/v) SDS, 1%(v/v) Triton X-100, 10 mM MgCl2) with anti-proteases and anti-phosphatases (Sigma-Aldrich;St.Louis, MO). The tissue lysates were centrifuged for 30 minutes at 18000 g in a microfuge at 4ºC. Liver and White Adipose Tissue total protein lysates were subjected to sodium–dodecyl sulfate-polyacrylamide gels (SDS–PAGE), then electrotransferred on a PVDF membrane and probed successively with the following antibodies: Hormone sensitive lipase/HSL: (Abcam Cat# ab45422, RRID:AB_2135367) ; Phospho-HSL (Ser660) (Cell Signaling Technology Cat# 4126, RRID:AB_490997) ; Phospho-Acetyl-

CoA Carboxylase (Ser79) (Cell Signaling Technology Cat# 3661, RRID:AB_330337) ; Acetyl CoA Carboxylase 1 : (Millipore Cat# 04-322, RRID:AB_673047) ; Lipoprotein lipase (LPL Antibody (H-53)): (Santa Cruz Biotechnology Cat# sc-32885, RRID:AB_2234585) ; Fatty Acid Synthase antibody (FAS): (Abcam Cat# ab128870, RRID:AB_11143436) ; CPT1A: (Abcam Cat# ab128568, RRID:AB_11141632) ; GAPDH: (Millipore Cat# CB1001, RRID:AB_2107426) ; β-actin: (Sigma-Aldrich Cat# A2228, RRID:AB_47669) after incubating the membranes with 5% BSA blocking buffer. For protein detection we used horseradish-peroxidase-conjugated secondary antibodies (Dako Denmark, Glostrup, Denmark). Specific antigen-antibody bindings were visualized using chemiluminescence method according to the manufacturer´s instructions (Pierce ECL Western Blotting Substrate, Thermo Scientific, USA). Values were expressed in relation to β-actin or GAPDH protein levels.

Blood lipids determinations

Serum cholesterol levels (1001093, Spinreact), triglycerides levels (1001310, Spinreact), free fatty acids levels (436-91995, 434-91795, WAKO) were measured by spectrophotometry in a ThermoScientific Multiskan GO spectrophotometer.

Histomorphology of WAT

WAT samples were fixed in 10% formalin for 24h and then were dehydrated and embedded in paraffin. Sections of 3μm were made on a microtome and stained by the standard hematoxylin/eosin alcoholic (BioOptica, Italy) and sections were observed and photographed using a Provis AX70 microscope (Olympus, Corp, Tokyo, Japan). Digital images were quantified with *ImageJ Software* (National Institute of Health; USA).

Triglycerides content in liver

Approx. 500mg of livers were homogenized for 3min in ice-cold chloroform-methanol (2:1, vol/vol). Triglycerides were extracted during 3hours shaking at room temperature. For phase separation, mili-Q water was added. Samples were centrifuged and the organic bottom layer was recollected. The organic solvent was dried using a Speed Vac and re-dissolved in chloroform. Triglycerides content of the samples were measured after evaporation of the organic solvent (1001310, Spinreact) by spectrophotometry in a ThermoScientific Multiskan GO spectrophotometer.

Oil Red O Staining

Frozen sections of 8μm of liver were cut with a cryostat and stained in filtered oil Red O for 10 min. The sections were washed in distilled water, counterstained with Mayer´s hematoxylin for 3 min, and

mounted in aqueous mountant. Sections were observed and photographed using a Provis AX70 microscope (Olympus, Corp, Tokyo, Japan).

Primary cultures and cell lines experiments

Primary culture of tanycytes

Tanycytes were isolated from the median eminence of 10-day-old (P10) rats as described previously [54].

PamGene arrays

Primary cultures of tanycytes were incubated at 37°C with leptin (125nM) or DMSO for 2 or 15 minutes before washes and snap-freeze. For kinome analysis, STK microarrays were purchased from PamGene International BV (STK pamchips). Sample incubation, detection, and analysis were performed in a PamStation 12 according to the manufacturer's instructions and as previously described (Rabhi et al., 2018).

Fluorescent leptin internalization assay and immunofluorescence on primary culture

Tanycytes were seeded on poly-L-lysine-coated glass coverslips (10μg/ml) and incubated in TDM (DMEM/F-12 (#11039, ThermoFisher), 1% L-glutamine (#25030-024, ThermoFisher), 2% penicillin-streptomycin (#P4458, Sigma), insulin (1/1000, #I5500, Sigma), putrescin (1/500, #P5780, Sigma)) for 24 hours before the experiment. Tanycytes were incubated for the indicated amount of time at 37°C with either bioactive fluorescent leptin (Fluorescent-leptin, 125 nM, Cisbio Bioassays) or with fluorescent leptin antagonist (LAN, 125 nM, Cisbio Bioassays) both diluted in TDM. Cells were then fixed for 10min at 4°C with 4% paraformaldehyde (PFA, v/v in PBS) and washed 3 times with PBS 1X. For cointernalization assay, tanycytes were incubated with Fluorescent-leptin and XPA antibodies (30nM in TDM, Xoma Laboratories) for 5 min, washed and fixed. Cells were then washed and permeabilized with 0.1 % Triton-X100 (v/v in PBS) for 5 min at room temperature. Antibodies were all diluted in PBS with 3% BSA and incubated for 45 min at room temperature. Cells were either incubated with primary anti-EEA1 antibodies (1/200; Santa Cruz Biotechnology Cat# sc-6415, RRID:AB_2096822) followed by the Alexa488-conjugated anti-goat antibodies (1/1000; Molecular Probes Cat# A-11055, RRID:AB_2534102) or Alexa488-conjugated anti-human antibodies (1/1000; Molecular Probes Cat# A-11013, RRID:AB_141360) to stain XPA antibodies.

Fluorescent leptin release assay on primary culture

Tanycytes were incubated for 15 min at 37°C with either Fluorescent-leptin (125 nM, Cisbio Bioassays) or LAN (125 nM ; Cisbio Bioassays). Cells were washed with TDM, incubated with TDM for the indicated amount of time and fixed for 10 min at 4°C with 4% PFA. To assess the role of MAPK pathway, tanycytes were pre-incubated for 30 min with the MAPK inhibitor UO126 (10 μM in TDM; #9903; Cell signaling technology). Fluorescent-leptin uptake and release was performed in the presence of UO126. To check for LAN release with EGF, EGF-TRITC (10 ng/ml; #3481; Molecular probes) was added during the chase.

ELISA

To quantify leptin release, tanycytes were cultivated in 10 cm Petri dish and incubated with recombinant leptin (62.5 nM, Protein Rehovot Laboratory) diluted in TDM for 15 min at 37°C. Cells were then washed and incubated with TDM to chase leptin for the indicated amount of time. Leptin in the medium as well as leptin remaining in cells were quantified by Elisa assay according to the manufacturer's instruction (#MOB00 ; R&D systems). Leptin secretion was expressed as a percent of total leptin.

Image acquisition and analysis

Cells were observed under a confocal microscope TCS SP5 (Leica microsystems) and images were acquired according to Nyquist parameters using a 63x (NA 1.4) oil immersion objective. Single plane images were analyzed using the open source Icy software (http://icy.bioimageanalysis.org/). The cell periphery was manually delineated using phase contrast images and object-based segmentation using wavelet transform algorithm (spot detector plugin) was performed to detect vesicles in each channel. Objects were considered colocalized if the distance between their centroid was less than or equal to 3 pixels. EEA1 segmentation was used to estimate amounts of Leptin in EEA1 compartments and percent of total leptin in EEA1 determined by normalizing the integrated intensity of leptin in EEA1 to total leptin in cells.

Cells lines

HEK293T (human embryonic kidney), HeLa (cervical cancer), CHO (Chinese hamster ovary) and N46 hypothalamic cells were grown in DMEM (Dulbecco's modified Eagle's medium; Gibco, life

technologies) with 4500 mg/l glucose and 10% fetal calf serum (Invitrogen) in a 10% CO2 humidified atmosphere at 37°C. HEK293T cells were transiently transfected (48h) with jetPEI (Polyplus-transfection), with a mock pCDNA3 vector or LepR or EGFR expressing pCDNA3 plasmids, or with LIFR- or IL6R-expressing pMET7 plasmids. Activation of the ERK signaling pathway was performed in transfected HEK29T cells expressing exogenous EGFR, LepRb or both receptors, with or without a 1h pretreatment with 1μM AG1478 inhibitor (T4182, Sigma) prior to 15min of stimulation with EGF (1nM), Leptin (10nM) or both.

Western Blot on primary cultures and cell lines

The sequences and protocols for the preparation of the extracellular sub-domains of LepR have been described previously by us [80]. Cell lysates (in Laemmli buffer supplemented with 30mM DTT, 2mM orthovanadate and 10mM NaF) were separated by SDS/PAGE, transferred to nitrocellulose membranes and immunoblotted with anti-phospho-tyrosine (Tyr-705) STAT3 (Cell Signaling Technology Cat# 9145, RRID:AB_2491009) and anti-STAT3 antibodies (Cell Signaling Technology Cat# 9139, RRID:AB_331757), anti-phospho-tyrosine (Tyr-204) ERK1/2 (Santa Cruz Biotechnology Cat# sc-16982, RRID:AB_2139990) and anti-ERK2 (Proteintech Cat# 51068-1-AP, RRID:AB_2250380) antibodies, anti-FLAG tag (Sigma-Aldrich Cat# SAB4301135, RRID:AB_2811010), anti-HA tag (Cell Signaling Technology Cat#3724) or XPA (Xoma Laboratories). Western Blots were scanned on the Odyssey infra-red Imaging System (Licor).

Co-Immunoprecipitation

HEK293T cells were transfected with a Flag-EGFR-expressing vector either with LepR-YFP or an empty vector. 48h later, cells were harvested in lysis buffer containing Tris-EDTA-magnesium-1% Triton X-100 and solubilized for 2 hr (4°C, under rotation), centrifuged (14,000× *g*, 45 min), and supernatants were subjected to immunoprecipitation with 2 μg of antibody anti-GFP (Roche); 4 hr, 4°C, under rotation. Protein G beads (Sigma-Aldrich) were then added, and after a 2 hr incubation, the samples were washed in the 0.1% Triton X-100 buffer by repeated centrifugation (1,000× *g*, 5 min). The remaining pellet was resuspended in Laemmli buffer (62.5-mM Tris/HCl pH 6.8, 5% SDS, 10% glycerol, and 0.005% bromophenol blue), denaturated by heating (95°C, 5 min), and subjected to SDS-PAGE analysis.

Bioluminescence resonance energy transfer (BRET)-based LepR biosensor

HEK293T cells were transiently transfected in 12-well plates with 40 ng of LepR-Luciferase plasmid with increasing amounts of LepR-YFP plasmids. Cells were grown overnight and transferred into 96-well-Optiplates (PerkinElmer Life Sciences), pre-coated with 10 µg/mL poly-l-lysine (Sigma), where they were grown for additional 24 h. The next day cells were stimulated with leptin, XPA or vehicle for 30min at 37°C. After washing with PBS, Coelenterazine (Interchim France), a Luciferase substrate was added and cells were subjected to measurement of emission at Luciferase and YFP wavelength on a plate reader Tecan F500 (Tecan; Männedorf, Switzerland).

TR-FRET binding assay

TR-FRET assays are based on the energy transfer between a fluorescently labeled donor molecule (the long-lived fluorophore Terbium cryptate (Tb)) and a fluorescently labeled acceptor (d2). In order to covalently label cell surface EGFR or LepR, with the Tb, the receptor is fused to the SNAP enzyme that can be covalently labeled with the Tb fluorophore at a stoichiometry of 1Tb per 1SNAP-receptor, using a suicide enzyme substrate-Tb. 48 hours post-transfection, HEK293T cells, expressing SNAP-EGFR +LepR or SNAP-LepR +EGFR, and previously plated in P96-well plates pre-coated with 10 µg/mL poly-l-lysine (Sigma), are incubated with 100 nM of Tb-SNAP substrate in Tag-lite labeling medium (Cisbio Bioassays; 1h, 4°C). After several washes, cells are treated with several doses of leptin-d2 or EGF-d2 (CisbioAssays) respectively. For each concentration, non-specific binding was determined by adding an excess of unlabeled leptin or unlabeled EGF (200-500nM). Regarding the binding data analysis, the *B*max signal and the equilibrium dissociation constant (K_D) values were obtained by fitting the specific binding data points (triplicate) with one-binding site model using the GraphPad Prism software (GraphPad Software, Inc., San Diego, CA).

Statistics

Results are given as mean ± standard error mean (SEM). Samples or animals were excluded whether their values were outside the ± 2-fold standard deviation, or whether an objective experimental failure was observed; studies were not blinded to investigators or formally randomized. To test if the populations follow a Gaussian distribution, a normality test was performed (Kolgomorov-Smirnov test for n between 5-7; Shapiro-Wilk test for $n \geq 7$). For normal distributions, parametric test were used; for

two population comparisons, an unpaired t tests was used as indicated in figure legends[81-8381-8381-8380-8279-8178-8077-7976-7876-78]; for multiple comparison test, a one-way or two-way ANOVA followed by Tukey's *post hoc* multiple comparison test (unless otherwise indicated in the figure legends), was performed. For non-Gaussian distributions was used; Mann-Whitney test were used for two comparison test, and Kruskal-Wallis followed by Dunn *post hoc* test for multiple comparison. Data analysis was performed using GraphPad Prism Software Version 7 (GraphPad, San Diego, CA). The threshold for significance was $p<0,05$.

REFERENCES

1. Swinburn, B.A.*, et al.* The Global Syndemic of Obesity, Undernutrition, and Climate Change: The Lancet Commission report. *Lancet* **393**, 791-846 (2019).
2. Yoon, K.H.*, et al.* Epidemic obesity and type 2 diabetes in Asia. *Lancet* **368**, 1681-1688 (2006).
3. Ohn, J.H.*, et al.* 10-year trajectory of beta-cell function and insulin sensitivity in the development of type 2 diabetes: a community-based prospective cohort study. *Lancet Diabetes Endocrinol* **4**, 27-34 (2016).
4. Ahima, R.S. & Flier, J.S. Leptin. *Annu Rev Physiol* **62**, 413-437 (2000).
5. de Luca, C.*, et al.* Complete rescue of obesity, diabetes, and infertility in db/db mice by neuron-specific LEPR-B transgenes. *J Clin Invest* **115**, 3484-3493 (2005).
6. Cohen, P.*, et al.* Selective deletion of leptin receptor in neurons leads to obesity. *J.Clin.Invest* **108**, 1113-1121 (2001).
7. Caron, A., Lee, S., Elmquist, J.K. & Gautron, L. Leptin and brain-adipose crosstalks. *Nat Rev Neurosci* **19**, 153-165 (2018).
8. Pan, W.W. & Myers, M.G., Jr. Leptin and the maintenance of elevated body weight. *Nat Rev Neurosci* **19**, 95-105 (2018).
9. Friedman, J.M. Leptin and the endocrine control of energy balance. *Nature Metabolism* **1**, 754-764 (2019).
10. Kamohara, S., Burcelin, R., Halaas, J.L., Friedman, J.M. & Charron, M.J. Acute stimulation of glucose metabolism in mice by leptin treatment. *Nature* **389**, 374-377 (1997).
11. Coppari, R.*, et al.* The hypothalamic arcuate nucleus: a key site for mediating leptin's effects on glucose homeostasis and locomotor activity. *Cell Metab* **1**, 63-72 (2005).
12. Buettner, C.*, et al.* Critical role of STAT3 in leptin's metabolic actions. *Cell Metab* **4**, 49-60 (2006).
13. Buettner, C.*, et al.* Leptin controls adipose tissue lipogenesis via central, STAT3-independent mechanisms. *Nat Med* **14**, 667-675 (2008).
14. Prevot, V.*, et al.* The Versatile Tanycyte: A Hypothalamic Integrator of Reproduction and Energy Metabolism. *Endocr Rev* **39**, 333-368 (2018).
15. Garcia-Caceres, C.*, et al.* Role of astrocytes, microglia, and tanycytes in brain control of systemic metabolism. *Nat Neurosci* **22**, 7-14 (2019).
16. Banks, W.A. The blood-brain barrier as an endocrine tissue. *Nat Rev Endocrinol* **15**, 444-455 (2019).
17. Schaeffer, M.*, et al.* Rapid sensing of circulating ghrelin by hypothalamic appetite-modifying neurons. *Proc Natl Acad Sci U S A* **110**, 1512-1517 (2013).
18. Ciofi, P.*, et al.* Brain-endocrine interactions: a microvascular route in the mediobasal hypothalamus. *Endocrinology* **150**, 5509-5519 (2009).
19. Yulyaningsih, E.*, et al.* Acute Lesioning and Rapid Repair of Hypothalamic Neurons outside the Blood-Brain Barrier. *Cell Rep* **19**, 2257-2271 (2017).
20. Djogo, T.*, et al.* Adult NG2-Glia Are Required for Median Eminence-Mediated Leptin Sensing and Body Weight Control. *Cell Metab* **23**, 797-810 (2016).

21. Mullier, A., Bouret, S.G., Prevot, V. & Dehouck, B. Differential distribution of tight junction proteins suggests a role for tanycytes in blood-hypothalamus barrier regulation in the adult mouse brain. *J Comp Neurol* **518**, 943-962 (2010).
22. Langlet, F.*, et al.* Tanycytic VEGF-A Boosts Blood-Hypothalamus Barrier Plasticity and Access of Metabolic Signals to the Arcuate Nucleus in Response to Fasting. *Cell Metab* **17**, 607-617 (2013).
23. Balland, E.*, et al.* Hypothalamic tanycytes are an ERK-gated conduit for leptin into the brain. *Cell Metab* **19**, 293-301 (2014).
24. Yuan, X., Caron, A., Wu, H. & Gautron, L. Leptin Receptor Expression in Mouse Intracranial Perivascular Cells. *Front Neuroanat* **12**, 4 (2018).
25. Yoo, S., Cha, D., Kim, D.W., Hoang, T.V. & Blackshaw, S. Tanycyte-Independent Control of Hypothalamic Leptin Signaling. *Front Neurosci* **13**, 240 (2019).
26. Bhaskar, V.*, et al.* An allosteric antibody to the leptin receptor reduces body weight and reverses the diabetic phenotype in the Lep(ob) /Lep(ob) mouse. *Obesity (Silver Spring)* **24**, 1687-1694 (2016).
27. Jo, Y.H., Chen, Y.J., Chua, S.C., Jr., Talmage, D.A. & Role, L.W. Integration of endocannabinoid and leptin signaling in an appetite-related neural circuit. *Neuron* **48**, 1055-1066 (2005).
28. Irani, B.G., Le Foll, C., Dunn-Meynell, A. & Levin, B.E. Effects of leptin on rat ventromedial hypothalamic neurons. *Endocrinology* **149**, 5146-5154 (2008).
29. Kusumakshi, S.*, et al.* A Binary Genetic Approach to Characterize TRPM5 Cells in Mice. *Chem Senses* **40**, 413-425 (2015).
30. Niv-Spector, L.*, et al.* Identification of the hydrophobic strand in the A-B loop of leptin as major binding site III: implications for large-scale preparation of potent recombinant human and ovine leptin antagonists. *Biochem J* **391**, 221-230 (2005).
31. Muller-Fielitz, H.*, et al.* Tanycytes control the hormonal output of the hypothalamic-pituitary-thyroid axis. *Nat Commun* **8**, 484 (2017).
32. Frayling, C., Britton, R. & Dale, N. ATP-mediated glucosensing by hypothalamic tanycytes. *J Physiol* **589**, 2275-2286 (2011).
33. Auriau, J.*, et al.* Gain of affinity for VEGF165 binding within the VEGFR2/NRP1 cellular complex detected by an HTRF-based binding assay. *Biochem Pharmacol* **158**, 45-59 (2018).
34. Vauthier, V.*, et al.* Design and validation of a homogeneous time-resolved fluorescence-based leptin receptor binding assay. *Anal Biochem* **436**, 1-9 (2013).
35. Langlet, F., Mullier, A., Bouret, S.G., Prevot, V. & Dehouck, B. Tanycyte-like cells form a blood-cerebrospinal fluid barrier in the circumventricular organs of the mouse brain. *J Comp Neurol* **521**, 3389-3405 (2013).
36. Howard, J.K. & Flier, J.S. Attenuation of leptin and insulin signaling by SOCS proteins. *Trends Endocrinol Metab* **17**, 365-371 (2006).
37. Chmielewski, A.*, et al.* Preclinical Assessment of Leptin Transport into the Cerebrospinal Fluid in Diet-Induced Obese Minipigs. *Obesity (Silver Spring)* **27**, 950-956 (2019).
38. Balland, E., Chen, W., Tiganis, T. & Cowley, M.A. Persistent leptin signalling in the arcuate nucleus impairs hypothalamic insulin signalling and glucose homeostasis in obese mice. *Neuroendocrinology* (2019).
39. Sukumaran, S., Xue, B., Jusko, W.J., Dubois, D.C. & Almon, R.R. Circadian variations in gene expression in rat abdominal adipose tissue and relationship to physiology. *Physiol Genomics* **42A**, 141-152 (2010).
40. Tschop, M., Smiley, D.L. & Heiman, M.L. Ghrelin induces adiposity in rodents. *Nature* **407**, 908-913 (2000).
41. Schwartz, M.W.*, et al.* Specificity of leptin action on elevated blood glucose levels and hypothalamic neuropeptide Y gene expression in ob/ob mice. *Diabetes* **45**, 531-535 (1996).
42. Pelleymounter, M.A.*, et al.* Effects of the obese gene product on body weight regulation in ob/ob mice. *Science* **269**, 540-543 (1995).
43. Berglund, E.D.*, et al.* Direct leptin action on POMC neurons regulates glucose homeostasis and hepatic insulin sensitivity in mice. *J Clin Invest* **122**, 1000-1009 (2012).
44. Back, S.H. & Kaufman, R.J. Endoplasmic reticulum stress and type 2 diabetes. *Annu Rev Biochem* **81**, 767-793 (2012).
45. Sohn, J.W.*, et al.* Melanocortin 4 receptors reciprocally regulate sympathetic and parasympathetic preganglionic neurons. *Cell* **152**, 612-619 (2013).
46. Muzumdar, R.*, et al.* Physiologic effect of leptin on insulin secretion is mediated mainly through central mechanisms. *FASEB J* **17**, 1130-1132 (2003).

47. Fagerholm, V., Haaparanta, M. & Scheinin, M. alpha2-adrenoceptor regulation of blood glucose homeostasis. *Basic Clin Pharmacol Toxicol* **108**, 365-370 (2011).
48. Rosengren, A.H.*, et al.* Overexpression of alpha2A-adrenergic receptors contributes to type 2 diabetes. *Science* **327**, 217-220 (2010).
49. Wang, P.*, et al.* A leptin-BDNF pathway regulating sympathetic innervation of adipose tissue. *Nature* **583**, 839-844 (2020).
50. Ahima, R.S.*, et al.* Role of leptin in the neuroendocrine response to fasting. *Nature* **382**, 250-252 (1996).
51. Zhou, Y.*, et al.* Temporal dynamic reorganization of 3D chromatin architecture in hormone-induced breast cancer and endocrine resistance. *Nat Commun* **10**, 1522 (2019).
52. Liu, Z.*, et al.* Short-term tamoxifen treatment has long-term effects on metabolism in high-fat diet-fed mice with involvement of Nmnat2 in POMC neurons. *FEBS Lett* **592**, 3305-3316 (2018).
53. Shida, D., Kitayama, J., Mori, K., Watanabe, T. & Nagawa, H. Transactivation of epidermal growth factor receptor is involved in leptin-induced activation of janus-activated kinase 2 and extracellular signal-regulated kinase 1/2 in human gastric cancer cells. *Cancer Res* **65**, 9159-9163 (2005).
54. Prevot, V., Cornea, A., Mungenast, A., Smiley, G. & Ojeda, S.R. Activation of erbB-1 signaling in tanycytes of the median eminence stimulates transforming growth factor beta1 release via prostaglandin E2 production and induces cell plasticity. *J.Neurosci.* **23**, 10622-10632 (2003).
55. Lomniczi, A., Cornea, A., Costa, M.E. & Ojeda, S.R. Hypothalamic tumor necrosis factor-alpha converting enzyme mediates excitatory amino acid-dependent neuron-to-glia signaling in the neuroendocrine brain. *J.Neurosci.* **26**, 51-62 (2006).
56. Balthasar, N.*, et al.* Leptin receptor signaling in POMC neurons is required for normal body weight homeostasis. *Neuron* **42**, 983-991 (2004).
57. van de Wall, E.*, et al.* Collective and individual functions of leptin receptor modulated neurons controlling metabolism and ingestion. *Endocrinology* **149**, 1773-1785 (2008).
58. Vauthier, V.*, et al.* Endospanin1 affects oppositely body weight regulation and glucose homeostasis by differentially regulating central leptin signaling. *Mol Metab* **6**, 159-172 (2017).
59. Obici, S.*, et al.* Central melanocortin receptors regulate insulin action. *J Clin Invest* **108**, 1079-1085 (2001).
60. Fan, W.*, et al.* The central melanocortin system can directly regulate serum insulin levels. *Endocrinology* **141**, 3072-3079 (2000).
61. Rossi, J.*, et al.* Melanocortin-4 receptors expressed by cholinergic neurons regulate energy balance and glucose homeostasis. *Cell Metab* **13**, 195-204 (2011).
62. Coppari, R. & Bjorbaek, C. Leptin revisited: its mechanism of action and potential for treating diabetes. *Nat Rev Drug Discov* **11**, 692-708 (2012).
63. Zamboni, M., Mazzali, G., Fantin, F., Rossi, A. & Di Francesco, V. Sarcopenic obesity: a new category of obesity in the elderly. *Nutr Metab Cardiovasc Dis* **18**, 388-395 (2008).
64. Parr, E.B., Coffey, V.G. & Hawley, J.A. 'Sarcobesity': a metabolic conundrum. *Maturitas* **74**, 109-113 (2013).
65. Tian, S. & Xu, Y. Association of sarcopenic obesity with the risk of all-cause mortality: A meta-analysis of prospective cohort studies. *Geriatr Gerontol Int* **16**, 155-166 (2016).
66. Okun, J.G., Rusu, P.M., Chan, A.Y. et al. . Liver alanine catabolism promotes skeletal muscle atrophy and hyperglycaemia in type 2 diabetes. *Nat Metab* **3**, 394-409 (2021).
67. Prentki, M. & Nolan, C.J. Islet beta cell failure in type 2 diabetes. *J Clin Invest* **116**, 1802-1812 (2006).
68. Steil, G.M.*, et al.* Adaptation of beta-cell mass to substrate oversupply: enhanced function with normal gene expression. *Am J Physiol Endocrinol Metab* **280**, E788-796 (2001).
69. Tuomi, T.*, et al.* The many faces of diabetes: a disease with increasing heterogeneity. *Lancet* **383**, 1084-1094 (2014).
70. Morimoto, A.*, et al.* Impact of impaired insulin secretion and insulin resistance on the incidence of type 2 diabetes mellitus in a Japanese population: the Saku study. *Diabetologia* **56**, 1671-1679 (2013).
71. Cohen, P.*, et al.* Selective deletion of leptin receptor in neurons leads to obesity. *J Clin Invest* **108**, 1113-1121 (2001).
72. Peitz, M., Pfannkuche, K., Rajewsky, K. & Edenhofer, F. Ability of the hydrophobic FGF and basic TAT peptides to promote cellular uptake of recombinant Cre recombinase: a tool for efficient genetic engineering of mammalian genomes. *Proc Natl Acad Sci U S A* **99**, 4489-4494 (2002).

73. Folgueira, C.*, et al.* Hypothalamic dopamine signaling regulates brown fat thermogenesis. *Nat Metab* **1**, 811-829 (2019).
74. Quinones, M.*, et al.* Sirt3 in POMC neurons controls energy balance in a sex- and diet-dependent manner. *Redox Biol* **41**, 101945 (2021).
75. Bruss, M.D., Khambatta, C.F., Ruby, M.A., Aggarwal, I. & Hellerstein, M.K. Calorie restriction increases fatty acid synthesis and whole body fat oxidation rates. *Am J Physiol Endocrinol Metab* **298**, E108-116 (2010).
76. Imbernon, M.*, et al.* Central melanin-concentrating hormone influences liver and adipose metabolism via specific hypothalamic nuclei and efferent autonomic/JNK1 pathways. *Gastroenterology* **144**, 636-649 e636 (2013).
77. Nogueiras, R.*, et al.* The central melanocortin system directly controls peripheral lipid metabolism. *J Clin Invest* **117**, 3475-3488 (2007).
78. Golde, W.T., Gollobin, P. & Rodriguez, L.L. A rapid, simple, and humane method for submandibular bleeding of mice using a lancet. *Lab Anim (NY)* **34**, 39-43 (2005).
79. Clasadonte, J., Scemes, E., Wang, Z., Boison, D. & Haydon, P.G. Connexin 43-Mediated Astroglial Metabolic Networks Contribute to the Regulation of the Sleep-Wake Cycle. *Neuron* **95**, 1365-1380 e1365 (2017).
80. Zabeau, L.*, et al.* Selection of non-competitive leptin antagonists using a random nanobody-based approach. *Biochem J* **441**, 425-434 (2012).
81. Student. The probable error of a mean. *Biometrika* **6**, 1-25 (1908).
82. Fay, D.S. & Gerow, K. A biologist's guide to statistical thinking and analysis (). *WormBook : the online review of C. elegans biology*, 10.1895/wormbook.1891.1159.1891 (2013).
83. Charan, J. & Biswas, T. How to Calculate Sample Size for Different Study Designs in Medical Research? *Indian Journal of Psychological Medicine* **35**, 121-126 (2013).

ACKNOWLEDGMENTS

This work was supported by the Agence National de la Recherche (ANR, France) Grant ANR-15-CE14-0025 to VP, RJ and SG, « European Genomic Institute for Diabetes » (E.G.I.D, ANR-10-LABX-46 to JSA and VP), DISTALZ (ANR-11-LABX-0009 to VP), BETAPLASTICITY, ANR-17-CE14-0034 to JSA, Université de Lille (to MD, CB and JSA), Fondation pour la Recherche Médicale (FRM, to MD), European Foundation for the Study of Diabetes (EFSD, to JSA), the European Research Council (ERC) Synergy Grant-2019-WATCH-810331 to V.P., R. N. and M. S, the “Who am I?” laboratory of excellence No.ANR-11-LABX-0071 (to JD), the DHU Autoimmune and Hormonal Diseases (Authors) (JD), the H2020-MSCA-IF-2016 grant GLUCOTANYCYTES_748134 to MI and the NIH grant R01DK123002 to Y-BK and VP. We thank Laure Rolland for excellent technical help with immunofluorescence analysis of pancreatic sections. We thank Yann Lepage and the UMS2014-US41 for their technical support.

AUTHORS CONTRIBUTIONS

M.D., C.F., C.B., M.M., A.S., J.C., M.I., D.F., I.M.-C., S.K., E.C., E.I., N.J., A.O. and S.O carried out the experiments. M.M., J.T., E.T., M.S., S.K. and U.B. generated tools, vectors and animal models. Y.-B.K., R.J., M.S., U.B, R.N., J.-S.A., S.G., J.D. and V.P. designed and planned the study. All authors contributed to the preparation of the manuscript.

COMPETING INTERETS

The authors declare no competing interest.

1247
1248
1249

FIGURES

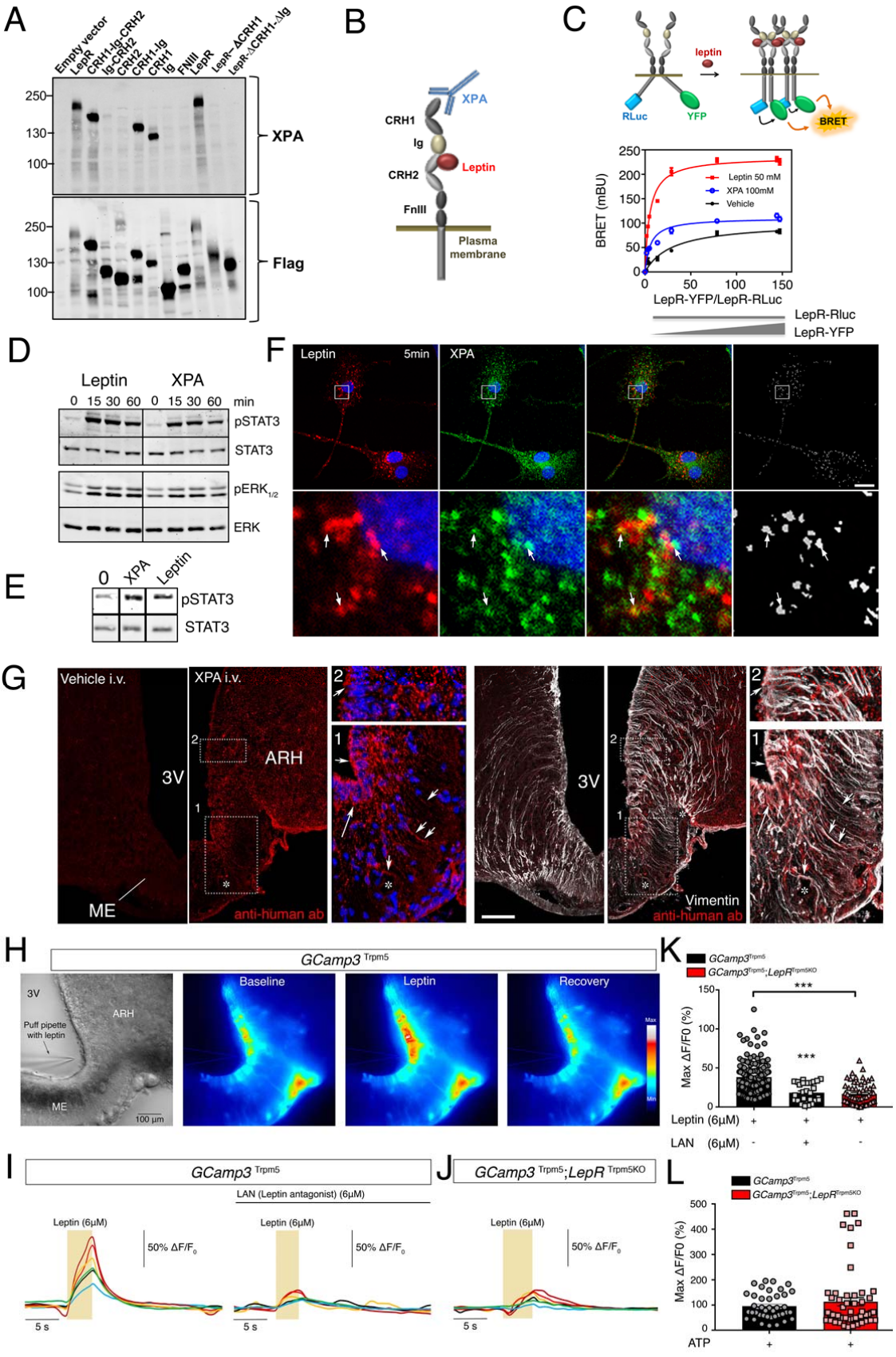
A
Empty vector
LepR
CRH1-Ig-CRH2
Ig-CRH2
CRH2
CRH1-Ig
CRH1
Ig
FNIII
LepR
LepR-ΔCRH1
LepR-ΔCRH1-ΔIg
250
130
100
XPA
Flag
B
XPA
CRH1
Ig
Leptin
CRH2
FnIII
Plasma membrane
C
leptin
RLuc
YFP
BRET
BRET (mBU)
Leptin 50 mM
XPA 100mM
Vehicle
LepR-YFP/LepR-RLuc
LepR-Rluc
LepR-YFP
D
Leptin
XPA
0 15 30 60 0 15 30 60 min
pSTAT3
STAT3
pERK1/2
ERK
E
0 XPA Leptin
pSTAT3
STAT3
F
Leptin 5min
XPA
G
Vehicle i.v.
XPA i.v.
3V
ARH
ME
anti-human ab
Vimentin
H
GCamp3 Trpm5
3V
ARH
Puff pipette with leptin
ME
100 µm
Baseline
Leptin
Recovery
Max
Min
K
GCamp3Trpm5
GCamp3Trpm5;LepRTrpm5KO
Max ΔF/F0 (%)
Leptin (6µM)
LAN (6µM)
I
GCamp3 Trpm5
LAN (Leptin antagonist) (6µM)
Leptin (6µM)
50% ΔF/F0
5 s
J
GCamp3 Trpm5;LepR Trpm5KO
L
ATP

Figure 1. Tanycytes of the median eminence express functional leptin receptors

(**A**) Western blot detection using the XPA antibody of different exogenously expressed LepR domains in HEK293 cells.

(**B**) Schematic representation of leptin receptor domains and the XPA binding site.

(**C**) *Top:* schematic representation of the BRET assay to study the ligand-induced conformational change/interaction between LepR-Rluc and LepR-YFP. *Bottom:* BRET donor saturation curves in HEK293T cells with a constant expression level of LepR-Rluc and increasing levels of LepR-YFP, upon stimulation with vehicle, leptin (50nM) or XPA (100nM) for 30 min at 37 °C.

(**D**) STAT3 and ERK1/2 phosphorylation in HEK293 cells stably expressing LepR after stimulation with 50 nM leptin or 100 nM XPA for 5, 15, 30 or 60 minutes.

(**E**) STAT3 phosphorylation in tanycytes upon 50 nM leptin or 100 nM XPA stimulation for 30 minutes.

(**F**) Leptin colocalizes with LepR in primary tanycytes. Representative confocal images of tanycytes treated for 5 min with 125 nM fluorescent leptin (red) together with 33 nM XPA antibodies against LepR labeled with fluorescent secondary antibodies (green). The extent of colocalization is represented by the mask on the right. Arrows point to examples of colocalized pixels. Scale bar: 10 µm.

(**G**) Representative photomicrograph revealing sites of XPA fixation in tanycytes of the median eminence (vimentin-positive cells) 2 minutes after intravenous XPA injection (2 nmol/animal) *in vivo*. White arrows show XPA (red) and vimentin (white) colocalization. 3V: third ventricle; ARH: arcuate nucleus of the hypothalamus; ME: median eminence. Scale bar: 200µm.

(**H**) Representative image of a living brain slice containing the median eminence from a *GCamp3*^{Trpm5} mouse under bright-field and fluorescence microscopy, showing the reversible increase in intracellular calcium levels in tanycytic cell bodies lining the third ventricle (3V) upon the local application of a puff of leptin (6µM) via a glass pipette. ME: median eminence. Scale bar: 100 µm

(**I**) Representative curves of GCamp3 fluorescence (calcium current) over time (Delta T) compared to the baseline in tanycytes in living hypothalamic slices during a puff of leptin (yellow rectangle, 6uM), alone (left curve) or after pre-treatment with leptin antagonist (LAN, 6µM, top black line; right curve), in a *GCamp3*^{Trpm5} mouse.

(**J**) Same measurement as in (**I**) in a *GCamp3*^{Trpm5}; *LepR*^{Trpm5} mouse lacking LepR in tanycytes after a puff of leptin (6µM, yellow rectangle).

(**K**) Graph representing maximum difference in calcium concentration from baseline during the treatment of living brain slices in *GCamp3*^{Trpm5} and *GCamp3*^{Trpm5}; *LepR*^{Trpm5} mice, described in (**I**) and (**J**). Mann Whitney test; ***: $p<0.001$; between indicated groups. Values indicate means ± SEM.

(**L**) Graph representing maximum c difference in calcium concentration from baseline during a puff of ATP (10 mM) in living brain slices from *GCamp3*^{Trpm5} and *GCamp3*^{Trpm5}; *LepR*^{Trpm5} mice. See also Supplementary Figure 1.

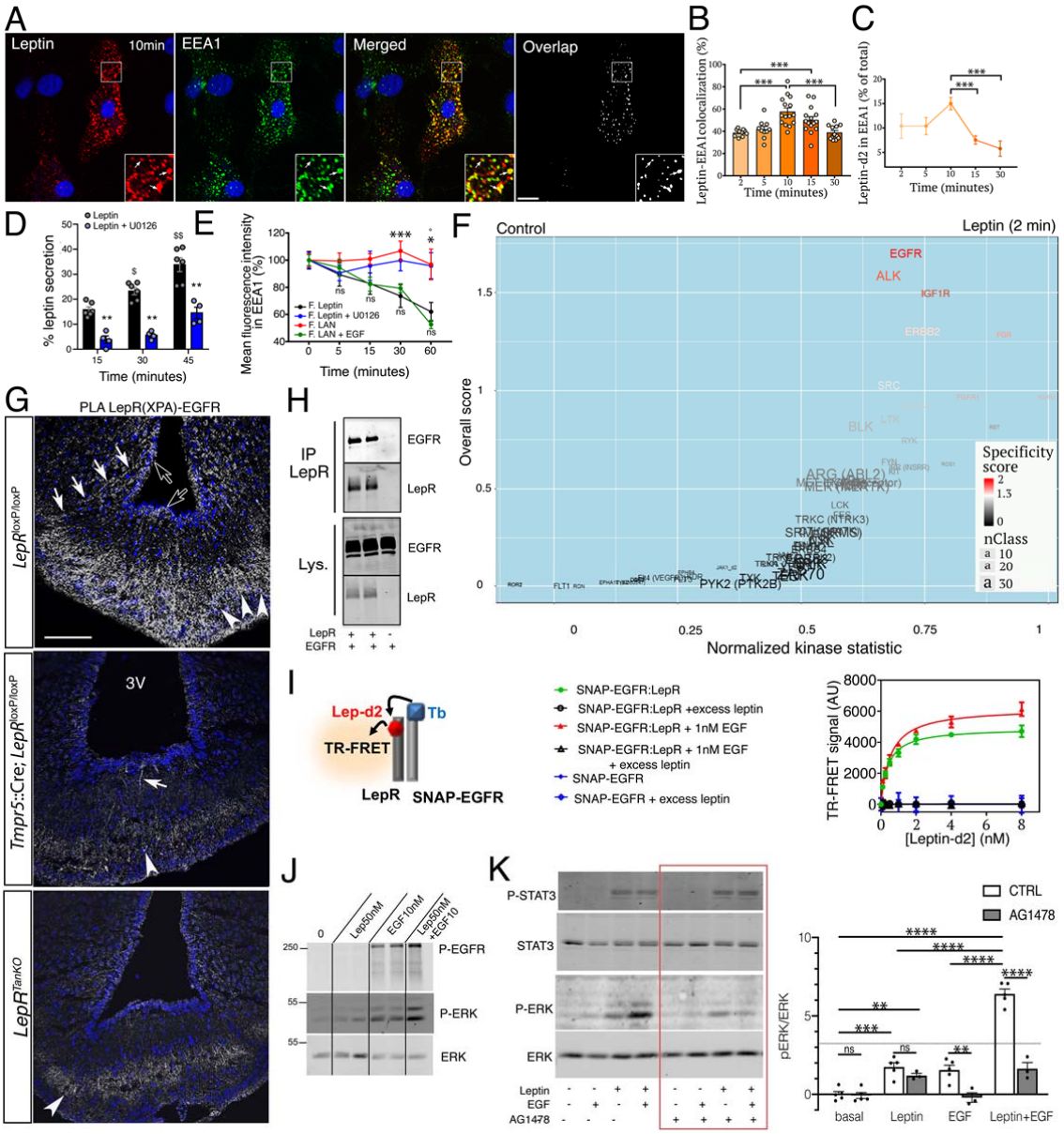

Figure 2. Tanycytic EGFR physically interacts with LepR in *vivo* and plays a role in leptin trancytosis *in vitro*

(**A**) Endocytosed leptin colocalizing with early endosomes. Representative confocal images showing primary tanycytes treated for 10 min with 125 nM fluorescent leptin (red) and antibodies to the early endosome marker EEA1 (green). The extent of colocalization is represented by the mask on the right. Arrows in inset point to examples of colocalized pixels. Scale bar: 10 µm.

(**B**) Percentage of leptin colocalizing with EEA1 over time following object-based detection of fluorescent leptin and EEA1 vesicles. Values represent means ± SEM. A Mann-Whitney test was applied. ***: p<0.001

(**C**) Percentage of endocytosed leptin found in the EEA1-positive compartment over time. Values represent means ± SEM. A Mann-Whitney test was applied. ***: p<0.001

(**D**) Leptin secreted into the medium by primary cultures of tanycytes as a percentage of total leptin concentration (intracellular and medium) 15, 30 and 45 minutes after fluorescent leptin addition. Mann-Whitney U test or one-way ANOVA as required. **: p<0.01 leptin vs. leptin + U0126; $: p<0.05 Leptin 15 min vs. Leptin 30 min and $$: p<0.01 Leptin 30 min vs. Leptin 45 min.

(**E**) Percentage (as % of 0 min time point) of endocytosed fluorescent leptin or fluorescent LAN found in EEA1 compartments over time in cells treated or not with U0126 (leptin) or EGF (LAN). Values represent means ± SEM. A Mann-Whitney U test was applied. ***: $p<0.001$

(**F**) Volcano plot showing differences in peptide phosphorylation between primary cultures of tanycytes treated for 2 min with vehicle (PBS pH 8.0) or leptin (1 µg/ml in PBS pH 8.0) (n=4). Upstream kinases were identified using the Human Protein Reference Database.

(**G**) Proximity Ligation Assay (PLA) between LepR and EGFR using XPA and a rabbit anti-EGFR antibody. PLA signal is seen in tanycytic cell bodies (empty arrows), processes (white arrows) and end-feet in the external zone of the median eminence, where they contact the fenestrated endothelium of the pituitary portal circulation (arrowheads). Scale bar: 100 µm.

(**H**) Co-immunoprecipitation of EGFR along with LepR in HEK293T cells; no co-immunoprecipitation of EGFR is observed when LepR is not expressed. IP, immunoprecipitation; Lys., cell lysate.

(**I**) Schematic representation of the TR-FRET technique (left). Right: specific saturation curves of leptin-d2 binding to its cognate receptor LepR within the LepR:SNAP-EGFR complex at the cell surface are obtained after 3h at 37°C; no TR-FRET signal is detected when SNAP-EGFR is expressed in the absence of LepR. Saturation binding experiments are performed by adding an increasing dose of leptin-d2, combined or not with 1nM EGF, to HEK293 cells expressing SNAP-EGFR alone or in combination with LepR and pre-labeled with the fluorescent SNAP-Tb substrate. The TR-FRET signal is strongly displaced by an excess of unlabeled leptin (200nM). Data are presented as means ± SD of 3 replicates of 1 representative experiment out of 3 independent experiments. The mean dissociation constant was determined from the average of the Kd values extracted from a fitting analysis of the saturation curve of 3 independent experiments with non-linear regression “one-site specific binding equation.

(**J**) Phosphorylation of EGFR and ERK upon addition of leptin 50nM, EGF 10nM or both for 30min at 37°C in primary tanycytes.

(**K**) Phosphorylation of STAT3 and ERK upon addition of leptin 10nM, EGF 1nM or both for 30min at 37°C in HEK293T cells expressing endogenous EGFR and transfected with LepRb in the presence or absence of the EGFR inhibitor AG1478 (1µM).

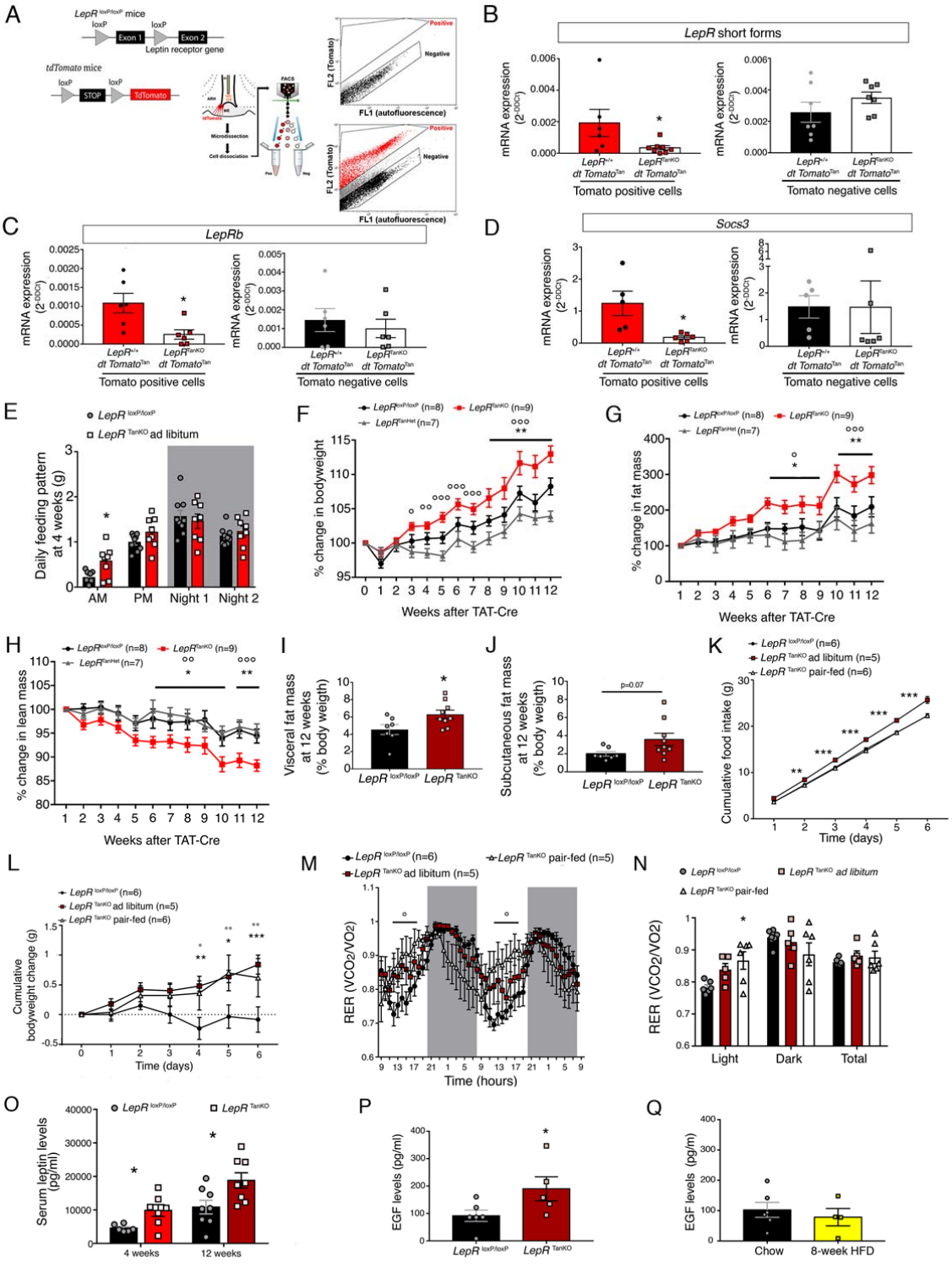

Figure 3. Selective LepR deletion in tanycytes causes food-intake-independent body weight gain and increased adiposity

(**A**) Schematic diagram and gating strategy for sorting Tomato positive cells following vehicle (top panel) and TAT-Cre infusion (bottom panel) into the third ventricle (3V) of *LepR*$^{+/+}$;*tdTomato*$^{\text{loxP-STOP-loxP}}$ or *LepR*$^{\text{loxP/loxP}}$;*tdTomato*$^{\text{loxP-STOP-loxP}}$ littermates.

(**B-D**) mRNA expression levels of short forms (**B**) and the long form, LepRb (**C**), of the leptin receptor, and of Socs3 (**D**) in tdTomato-positive cells (left panels) and tdTomato-negative cells (right panels). A Student t-test or Mann-Whitney U test was applied, depending on Shapiro-Wilk normality test results.*: p<0.05; $LepR^{+/+}$ $tdTomato^{Tan}$ vs. $LepR^{TanKO}$ $tdTomato^{Tan}$. Values indicate means ± SEM.

(**E**) Food intake pattern (daily average of automatic measurements in metabolic cages over 24h), showing an increase at lights-on in $LepR^{TanKO}$ mice when compared to $LepR^{loxP/loxP}$ littermates. *: p<0.05. Values indicate means ± SEM. The night was divided in two 6h time slots (Night 1 and Night 2).

(**F-H**) Curves representing the kinetics of the % change in body weight (**F**), % change in fat mass (**G**) and % change in lean mass (**H**) between $LepR^{loxP/loxP}$, $LepR^{TanHet}$ and $LepR^{TanKO}$ through the 12 weeks following the TAT-Cre infusion into the 3V. Two-way ANOVA with Tukey's correction; *: p<0.05, $LepR^{loxP/loxP}$ vs. $LepR^{TanKO}$; **: p<0.01, $LepR^{loxP/loxP}$ vs. $LepR^{TanKO}$; °: p<0.05, $LepR^{TanHet}$ vs. $LepR^{TanKO}$; °°: p<0.01, $LepR^{TanHet}$ vs. $LepR^{TanKO}$; °°°: p<0.05, $LepR^{TanHet}$ vs. $LepR^{TanKO}$. Values represent means ± SEM

(**I,J**) Visceral fat mass (**I**) and subcutaneous (**J**) 12 weeks after TAT-Cre infusion. Mann-Whitney U test; *: p<0.05, $LepR^{loxP/loxP}$ vs. $LepR^{TanKO}$. Values indicate means ± SEM.

(**K**) Cumulative food intake in $LepR^{TanKO}$ pair-fed mice 12 weeks after TAT-Cre infusion compared to their control littermates. 2-way ANOVA with Tukey's correction; **: p<0.01, $LepR^{loxP/loxP}$ and $LepR^{TanKO}$ pair-fed vs. $LepR^{TanKO}$ fed *ad libitum;* ***: p<0.001, $LepR^{loxP/loxP}$ and $LepR^{TanKO}$ pair-fed vs $LepR^{TanKO}$ *ad libitum.* Values indicate means ± SEM.

(**L**) Cumulative body weight change. 2-way ANOVA with Tukey's correction; *: p<0.05, $LepR^{loxP/loxP}$ vs. $LepR^{TanKO}$ fed *ad libitum*; **: p<0.01, $LepR^{loxP/loxP}$ vs. $LepR^{TanKO}$ fed *ad libitum;* ***: p<0.001, $LepR^{loxP/loxP}$ vs. $LepR^{TanKO}$ fed *ad libitum;* °: p< p<0.05, $LepR^{loxP/loxP}$ vs. $LepR^{TanKO}$ pair-fed; °°: p< p<0.01, $LepR^{loxP/loxP}$ vs. $LepR^{TanKO}$ pair-fed. Values indicate means ± SEM.

(**M**) Energy ratio (RER) over time. 2-way ANOVA with uncorrelated Fisher's LSD test; °: p< p<0.05, $LepR^{loxP/loxP}$ vs. $LepR^{TanKO}$ pair-fed. Values indicate means ± SEM.

(**N**) Mean energy ratio (RER) during light phase, dark phase and total.
Two-way ANOVA with Tukey's correction; *: p< p<0.05, $LepR^{loxP/loxP}$ vs. $LepR^{TanKO}$ pair-fed. Values indicate means ± SEM.

(**O**) Circulating leptin levels in $LepR^{loxP/loxP}$ and $LepR^{TanKO}$ animals at 4 weeks and 12 weeks after TAT-Cre infusion into the 3V. Mann-Whitney test (4 weeks) and unpaired t-test (12 weeks). *: p<0,05 $LepR^{loxP/loxP}$ vs. $LepR^{TanKO}$. Values represent means ± SEM.

(**P**) Basal serum EGF concentrations in $LepR^{loxP/loxP}$ and $LepR^{TanKO}$ mice, 12 weeks after TAT-Cre infusion. Mann-Whitney U test. *: p<0.05, $LepR^{loxP/loxP}$ vs. $LepR^{TanKO}$.

(**Q**) Basal serum EGF concentrations in C57Bl/6J mice fed normal chow or those fed a high-fat diet for 8 weeks.

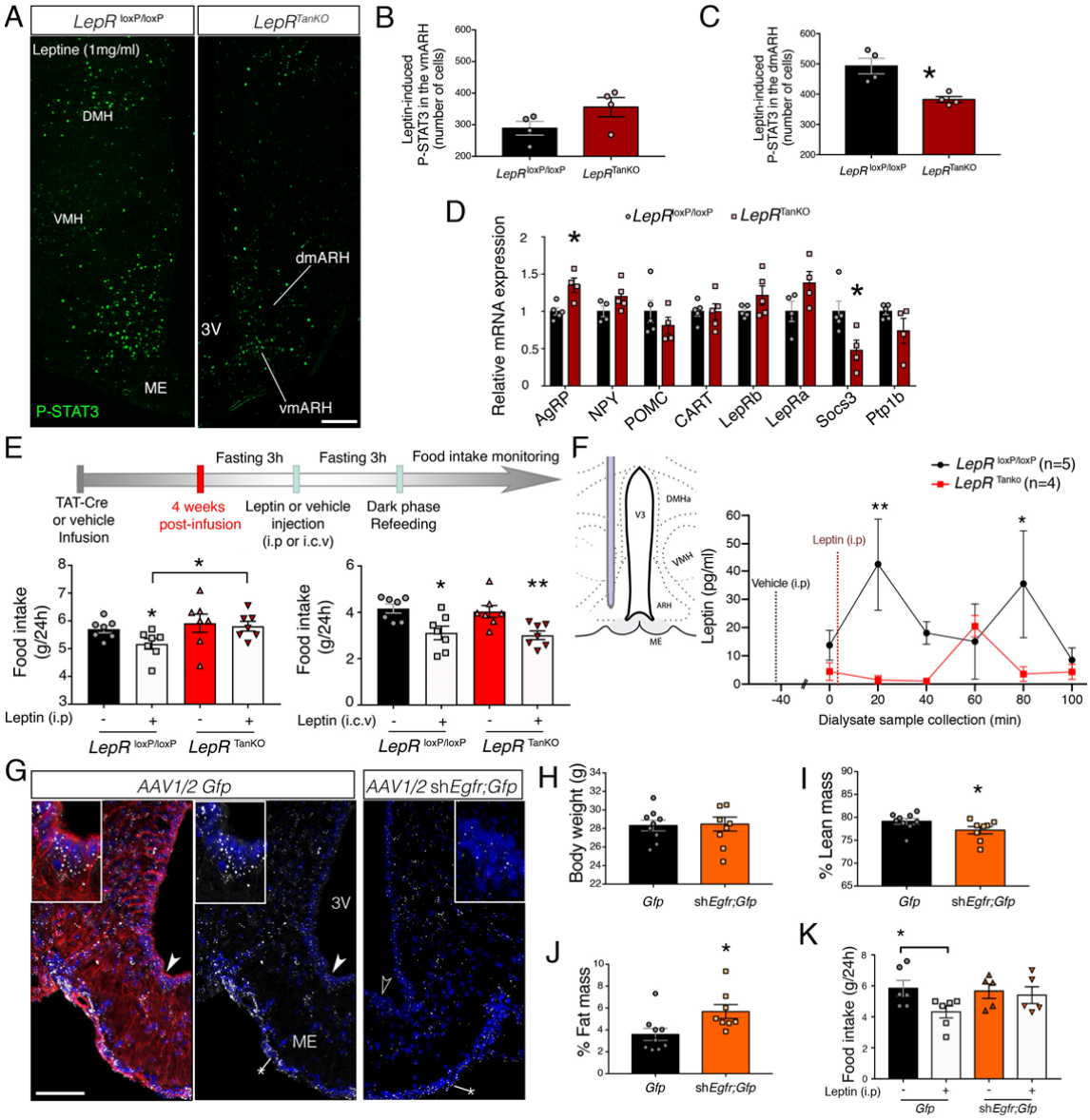

Figure 4. Defective LepR and EGFR signaling in tanycytes causes hypothalamic resistance to circulating leptin.

(**A-C**) Representative photomicrograph (**A**) and quantification of leptin-induced P-STAT3 immunofluorescence in the ventromedial (vm) (**B**) and dorsomedial (dm) arcuate nucleus (ARH) (**C**). Scale bar: 200µm. Unpaired Student's t-test. *: p<0.05 *LepR*$^{loxP/loxP}$ vs *LepR*$^{TanKO.}$ Values indicate means ± SEM.

(**D**) Relative mRNA expression levels of several genes known to be involved in the hypothalamic regulation of energy homeostasis and leptin activity in the microdissected mediobasal hypothalamus (MBH) of *LepR*$^{loxP/loxP}$ and *LepR*^{TanKO} mice, 12 weeks after TAT-Cre infusion. Student's t-test or Mann-Whitney U test, depending on Shapiro-Wilk normality test results. *: p<0.05, *LepR*$^{loxP/loxP}$ vs. *LepR*^{TanKO}. Values indicate means ± SEM.

(**E**) Schematic diagram showing the design of the experiment investigating the anorectic response to either intraperitoneal (i.p) or intracerebroventricular (i.c.v) leptin administration. Bottom left graph represents food intake in *LepR*$^{loxP/loxP}$ (black and grey bars) and *LepR*^{TanKO} mice (red and pink bars)

24h after i.p. leptin (3mg/kg, grey and pink bars) or vehicle (PBS pH 8.0, black and red bars) administration. Bottom right graph represents food intake in *LepR*$^{loxP/loxP}$ and *LepR*^{TanKO} mice 24h after i.c.v. leptin (2µg in 2µL) or vehicle (2µL PBS pH 8.0) injection. Mann-Whitney U test; *: $p<0.05$; **: $p<0.01$; leptin vs. vehicle and between indicated groups. Values indicate means ± SEM.

(**F**) Leptin concentrations in the ARH interstitial liquid collected by microdialysis every 20 minutes following i.p. vehicle ($t_{-40\ min}$) or leptin ($t_{-1\ min}$) injection in *LepR*$^{loxP/loxP}$ (n= 7) and *LepR*^{TanKO} mice (n=6). Two-way ANOVA followed by Fisher´s LSD post hoc test analysis was applied; *: p<0.05; **: p<0.01; *LepR*$^{loxP/loxP}$ vs. *LepR*^{TanKO}

(**G**) Representative photomicrograph of *in situ* hybridation of EGFR using RNAscpe technology on fresh-frozen brain sections from the median eminence of C57Bl/6J mice injected with *AAV1/2 Dio2::gfp* or *AAV(1+2)-GFP-U6-m-EGFR-shRNA*. The left panel shows vimentin-immunoreactivity in red. Arrowheads show the cells seen at higher magnification in insets. Scale bar: 100µm (25 µm in inset).

(**H-J**) Curves representing the evolution of body weight (**H**), % change in fat mass (**I**) and % change in lean mass (**J**) between mice injected with *AAV1/2 Dio2::gfp* (control in black) or *AAV(1+2)-GFP-U6-m-EGFR-shRNA* (in orange) over 4 weeks following the beginning of the viral activity. 2-way ANOVA with Tukey's correction; *: p<0.05, *AAV1/2 Gfp* vs. *AAV1/2 shEgfr.*

(**K**) Graph representing food intake in mice injected with *AAV1/2 Dio2::gfp* or *AAV(1+2)-GFP-U6-m-EGFR-shRNA* 24h after i.p. leptin (1mg/kg) or vehicle (PBS pH 8.0) injection. An unpaired Student's t-test was applied; *: p<0.05; **: p<0.01; leptin vs. vehicle and between indicated groups. Values indicate means ± SEM.

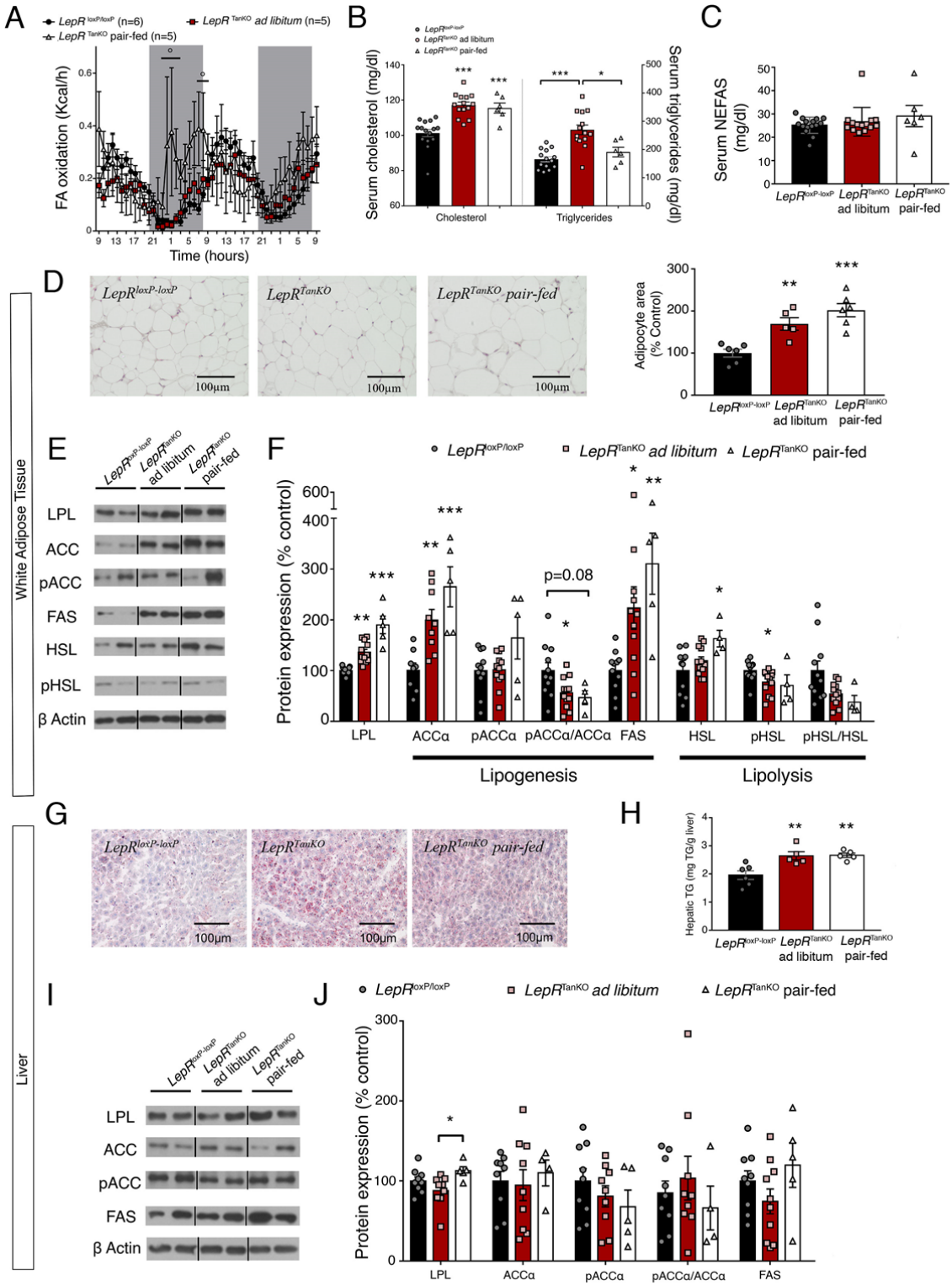

Figure 5: Selective LepR deletion in tanycytes causes hyperlipidemia and steatosis

(**A**) Fatty-acid (FA) oxidation over time. 2-way ANOVA with uncorrelated Fisher's LSD test; °: p< p<0.05, *LepR*$^{loxP/loxP}$ vs. *LepR*^{TanKO} pair-fed. Values indicate means ± SEM.

(**B**) Graphs representing serum cholesterol and triglyceride concentrations in *LepR*$^{loxP/loxP}$ and *LepR*^{TanKO} mice fed *ad libitum* on chow and *LepR*^{TanKO} mice pair-fed with *LepR*$^{loxP/loxP}$ mice, 12 weeks

after TAT-Cre infusion. One-way ANOVA with Tukey multiple comparison test or Kruskal-Wallis test with Dunn multiple comparison test were applied depending Shapiro-Wilk normality test results.. *: $p<0.05$; ***: $p<0.001$, $LepR^{TanKO}$ *ad libitum* or $LepR^{TanKO}$ pair fed vs. $LepR^{loxP/loxP}$ mice. Values indicate means ± SEM.

(**C**) Graph representing serum non-esterified fatty acid (NEFAS) concentrations in $LepR^{loxP/loxP}$ and $LepR^{TanKO}$ mice fed *ad libitum* on chow and $LepR^{TanKO}$ mice pair-fed with $LepR^{loxP/loxP}$ mice, 12 weeks after TAT-Cre infusion. One-way ANOVA with Tukey multiple comparison test *: $p<0.05$; ***: $p<0.001$, $LepR^{TanKO}$ *ad libitum* or $LepR^{TanKO}$ pair fed vs. $LepR^{loxP/loxP}$ mice. Values indicate means ± SEM.

(**D**) Representative images of histological hematoxylin-eosin staining of the adipose tissue in $LepR^{loxP/loxP}$ and $LepR^{TanKO}$ mice fed *ad libitum* on chow and $LepR^{TanKO}$ mice pair-fed with $LepR^{loxP/loxP}$ mice. Graph shows quantification of adipocyte size. One-way ANOVA with Tukey multiple comparison test. **: p<0.01, ***: p<0.001, $LepR^{TanKO}$ *ad libitum* or $LepR^{TanKO}$ pair fed vs. $LepR^{loxP/loxP}$ mice. Values indicate means ± SEM.

(**E**) Representative western blots of the different proteins mentioned in (**E**).

(**F**) Graph representing protein expression levels of several proteins implicated in fatty acid synthesis or fatty acid lipolysis in white adipose tissue from $LepR^{loxP/loxP}$ and $LepR^{TanKO}$ mice, 12 weeks after TAT-Cre infusion. Lipoprotein lipase (LPL) is implicated in the lipids uptake from the circulation to the adipose tissue. One-way ANOVA with Tukey multiple comparison test or Kruskal-Wallis test with Dunn multiple comparison test. *: $p<0.05$; ***: $p<0.001$, $LepR^{TanKO}$ *ad libitum* or $LepR^{TanKO}$ pair fed vs. $LepR^{loxP/loxP}$ mice. Values indicate means ± SEM.

(**G**) Representative Oil-Red-stained images from the liver of $LepR^{loxP/loxP}$ and $LepR^{TanKO}$ mice fed *ad libitum* and $LepR^{TanKO}$ mice pair-fed with $LepR^{loxP/loxP}$ mice.

(**H**) Quantification of triglycerides in the liver of $LepR^{loxP/loxP}$ and $LepR^{TanKO}$ mice fed *ad libitum* and $LepR^{TanKO}$ mice paired-fed with $LepR^{loxP/loxP}$ mice. One-way ANOVA with Tukey multiple comparison test. **: $p<0.01$, $LepR^{TanKO}$ *ad libitum* or $LepR^{TanKO}$ pair fed vs. $LepR^{loxP/loxP}$ mice. Values indicate means ± SEM.

(**I**) Representative western blots of the different proteins mentioned in (**I**).

(**J**) Graph representing protein expression levels of several proteins implicated in fatty acid synthesis and lipid uptake from the circulation into the liver in $LepR^{loxP/loxP}$ and $LepR^{TanKO}$ mice fed *ad libitum* and $LepR^{TanKO}$ mice paired-fed with $LepR^{loxP/loxP}$ mice, 12 weeks after TAT-Cre infusion. One-way ANOVA with Tukey multiple comparison test. *: $p<0.05$; $LepR^{TanKO}$ pair fed vs. $LepR^{TanKO}$ *ad libitum* mice. Values indicate means ± SEM.

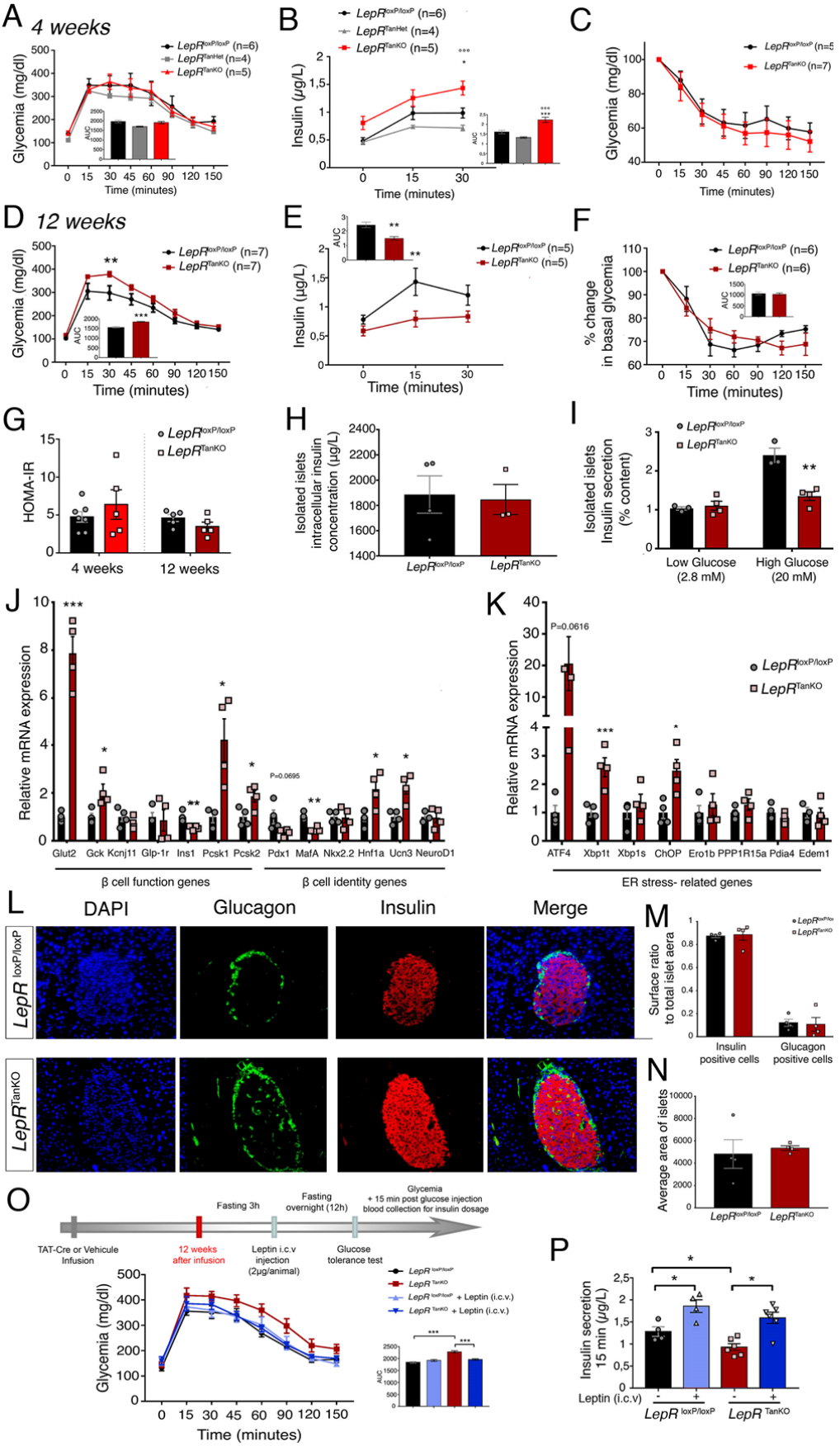
A
4 weeks
Glycemia (mg/dl)
Time (minutes)
B
Insulin (µg/L)
C
D
12 weeks
E
F
% change in basal glycemia
G
HOMA-IR
4 weeks
12 weeks
H
Isolated islets intracellular insulin concentration (µg/L)
I
Isolated islets Insulin secretion (% content)
Low Glucose (2.8 mM)
High Glucose (20 mM)
J
Relative mRNA expression
Glut2 Gck Kcnj11 Glp-1r Ins1 Pcsk1 Pcsk2 Pdx1 MafA Nkx2.2 Hnf1a Ucn3 NeuroD1
β cell function genes
β cell identity genes
K
P=0.0616
ATF4 Xbp1t Xbp1s ChOP Ero1b PPP1R15a Pdia4 Edem1
ER stress- related genes
L
DAPI
Glucagon
Insulin
Merge
M
Surface ratio to total islet aera
Insulin positive cells
Glucagon positive cells
N
Average area of islets
O
Fasting 3h
Fasting overnight (12h)
Glycemia + 15 min post glucose injection blood collection for insulin dosage
TAT-Cre or Vehicule Infusion
12 weeks after infusion
Leptin i.c.v injection (2µg/animal)
Glucose tolerance test
P
Insulin secretion 15 min (µg/L)
Leptin (i.c.v)

1471

Figure 6. Loss of LepR expression in median eminence tanycytes causes severe pancreatic β cell dysfunction possibly due to defective noradrenaline activity

(**A**) Curve representing glycemia during a glucose tolerance test in *LepR*$^{loxP/loxP}$, *LepR*^{TanHet} and *LepR*^{TanKO} mice, 4 weeks after TAT-Cre infusion. Graph represents the area under the curve; 2-way ANOVA with Tukey's correction. Values indicate means ± SEM.

(**B**) Serum insulin concentrations during the first 30 mins of a glucose tolerance test in *LepR*$^{loxP/loxP}$, *LepR*^{TanHet} and *LepR*^{TanKO} mice, 4 weeks after TAT-Cre infusion; 2-way ANOVA with Tukey's correction; *: p<0.05, *LepR*$^{loxP/loxP}$ vs. *LepR*^{TanKO} ; °°°: p<0.001, *LepR*^{TanHet} vs. *LepR*^{TanKO}. Graph represents the area under the curve; Student's t-test; ***: p<0.001, *LepR*$^{loxP/loxP}$ vs. *LepR*^{TanKO} ; °°°: p<0.001, *LepR*^{TanHet} vs. *LepR*^{TanKO}. Values indicate means ± SEM.

(**C**) Graph representing serum insulin concentrations at T0 of the glucose tolerance test; Student's t-test; *: p<0.05, *LepR*$^{loxP/loxP}$ vs *LepR*^{TanKO}. Values indicate means ± SEM.

(**D**) Curve representing glycemia during a glucose tolerance test in *LepR*$^{loxP/loxP}$ and *LepR*^{TanKO} mice, 12 weeks after TAT-Cre infusion; 2-way ANOVA with Tukey's correction; **: p<0.01, *LepR*$^{loxP/loxP}$ vs. *LepR*^{TanKO}. Graph represents the area under the curve; Student's t-test; ***: p<0.001, *LepR*$^{loxP/loxP}$ vs. *LepR*^{TanKO}. Values indicate means ± SEM.

(**E**) Serum insulin concentrations during the first 30 mins of a glucose tolerance test in *LepR*$^{loxP/loxP}$ and *LepR*^{TanKO} mice, 12 weeks after TAT-Cre infusion; 2-way ANOVA with Tukey's correction; **: p<0.01, *LepR*$^{loxP/loxP}$ vs *LepR*^{TanKO}. Graph represents the area under the curve; Student's t-test; **: p<0.01, *LepR*$^{loxP/loxP}$ vs. *LepR*^{TanKO}. Values indicate means ± SEM.

(**F**) Percentage change in basal glycemia during an insulin tolerance test in *LepR*$^{loxP/loxP}$ and *LepR*^{TanKO} mice, 12 weeks after TAT-Cre infusion. Values indicate means ± SEM.

(**G**) Graph representing insulin secretion from total isolated pancreatic islets from *LepR*$^{loxP/loxP}$ and *LepR*^{TanKO} mice, 12 weeks after TAT-Cre infusion, following treatment with low or high glucose concentrations. Student's t-test; **: p<0.01, *LepR*$^{loxP/loxP}$ vs. *LepR*^{TanKO}. Values indicate means ± SEM.

(**H**) Graph representing insulin concentrations in isolated pancreatic islets from *LepR*$^{loxP/loxP}$ and *LepR*^{TanKO} mice, 12 weeks after TAT-Cre infusion. Values indicate means ± SEM.

(**I**) Relative mRNA expression levels of markers of β cell function and identity in isolated pancreatic islets from *LepR*$^{loxP/loxP}$ and *LepR*^{TanKO} mice, 12 weeks after TAT-Cre infusion. A Student t-test or Mann-Whitney U test was applied, depending on Shapiro-Wilk normality test results. *: p<0.05, *LepR*$^{loxP/loxP}$ vs. *LepR*^{TanKO}. Values indicate means ± SEM.

(**J**) Relative mRNA expression levels of ER stress markers in isolated pancreatic islets from *LepR*$^{loxP/loxP}$ and *LepR*^{TanKO} mice, 12 weeks after TAT-Cre infusion. A Student t-test or Mann-Whitney U test was applied, depending on Shapiro-Wilk normality test results. *: p<0.05, *LepR*$^{loxP/loxP}$ vs. *LepR*^{TanKO}. Values indicate means ± SEM.

(**K**) Confocal images representing nuclei (blue), glucagon (green) and insulin (red) in isolated pancreatic islets from *LepR*$^{loxP/loxP}$ and *LepR*^{TanKO} mice, 12 weeks after TAT-Cre infusion.

(**L**) Graphs representing the ratio between insulin-positive (left) or glucagon-positive area (right) to the total islet surface area in *LepR*$^{loxP/loxP}$ and *LepR*^{TanKO} mice, 12 weeks after TAT-Cre infusion. Values indicate means ± SEM.

(**M**) Graph representing the average surface area of pancreatic islets from *LepR*$^{loxP/loxP}$ and *LepR*^{TanKO} mice, 12 weeks after TAT-Cre infusion. Values indicate means ± SEM.

(**N**) Graph representing serum noradrenaline concentrations in *LepR*$^{loxP/loxP}$ and *LepR*^{TanKO} mice, 12 weeks after TAT-Cre infusion. Student's t-test. *: p<0.05, *LepR*$^{loxP/loxP}$ vs. *LepR*^{TanKO}. Values indicate means ± SEM. Student's t-test; *: p<0.05

(**O**) Curve representing glycemia during a glucose tolerance test in *LepR*$^{loxP/loxP}$ and *LepR*^{TanKO} mice, before (black and red curves) and after (light and dark blue curves) i.c.v. leptin injection (2µg/animal). Graph represents the area under the curve; 1-way ANOVA with Tukey's correction; ***: p<0.001 between groups. Values indicate means ± SEM.

(**P**) Serum insulin concentrations at 15 minutes during the glucose tolerance test presented in (O). A paired Student's t-test was applied for comparisons between the same group before and after leptin

injection and an unpaired Student's t-test between *LepR*$^{loxP/loxP}$ and *LepR*^{TanKO} ; *: $p<0.05$. Values indicate means ± SEM.

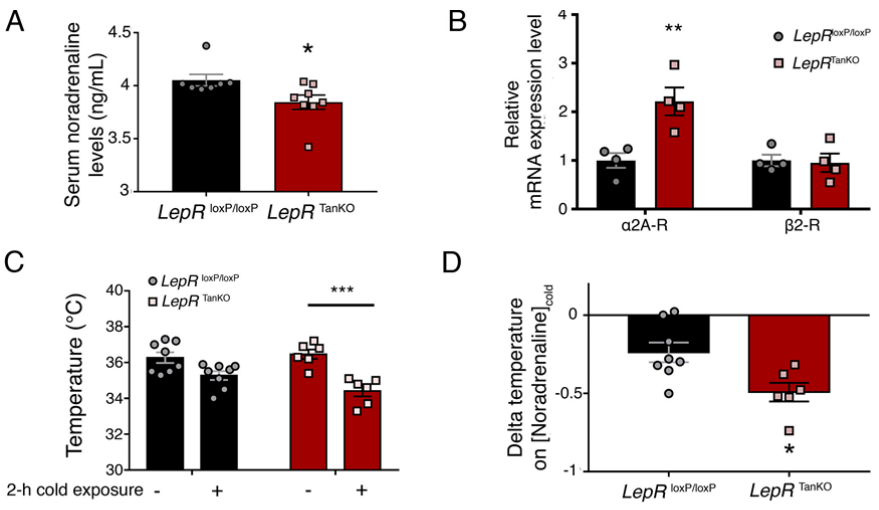

E

	$LepR^{loxP/loxP}$			$LepR^{TanKO}$		
	Fed	Fasting + Saline	Fasting + Leptin	Fed	Fasting + Saline	Fasting + Leptin
Blood glucose ($mg.dl^{-1}$)	215.8 ± 14.8	96.7 ± 1.9***	105.0 ± 4.7***	217.6 ± 7.5	97.4 ± 6.6***	107.0 ± 2.4***
Bodyweight change in fasting and refed mice (g/24h refeeding)		1.92 ± 0.18	1.33 ± 0.19$		1.08 ± 0.35	0.80 ± 0.37
Cumulative food intake in fasting and refed mice (g)						
4h		1.35 ± 0.06	1.15 ± 0.04$		1.28 ± 0.06	1.2 ± 0.08
12h		2.65 ± 0.13	2.07 ± 0.22$		2.22 ± 0.19	1.98 ± 0.12
24h		6.07 ± 0.29	5.30 ± 0.28		5.60 ± 0.57	4.94 ± 0.26
Corticosterone (ng.ml-1)	38.1 ± 2.6	88.0 ± 9.9***	58.9 ± 5.9*$$	40.5 ± 3.8	57.5 ± 10.3	51.4 ± 6.9

Figure 7. Loss of LepR expression in median eminence tanycytes impairs cold- and fasting-mediated increases in noradrenaline and corticosterone, respectively.

(**A**) Serum noradrenaline concentrations in *LepR*$^{loxP/loxP}$ and *LepR*^{TanKO} mice, 12 weeks after TAT-Cre infusion. Unpaired Student's t-test. *: p<0.05 *LepR*$^{loxP/loxP}$ vs. *LepR*^{TanKO}. Values indicate means ± SEM.

(**B**) Relative mRNA expression levels of adrenergic receptors in isolated pancreatic islets from *LepR*$^{loxP/loxP}$ and *LepR*^{TanKO} mice, 12 weeks after TAT-Cre infusion. Unpaired Student's t-test. **: p<0.01, *LepR*$^{loxP/loxP}$ vs. *LepR*^{TanKO}. Values indicate means ± SEM.

(**C**) Rectal temperature mesured in *LepR*$^{loxP/loxP}$ and *LepR*^{TanKO} mice, 12 weeks after TAT-Cre infusion, before and after 2h cold exposure. Paired Student's t-test. *** p<0.001 in *LepR*^{TanKO} before cold exposure vs. *LepR*^{TanKO} after cold exposure. Values indicate means ± SEM.

(**D**) Ratio between the delta temperature after-before cold exposure to the serum noradrenaline concentration after cold exposure from *LepR*$^{loxP/loxP}$ and *LepR*^{TanKO} mice. Unpaired Student's t-test. *: p<0.05, *LepR*$^{loxP/loxP}$ vs. *LepR*^{TanKO}. Values indicate means ± SEM.

(**E**) Table summarizing data from fed and 24h fasting and refed *LepR*$^{loxP/loxP}$ and *LepR*^{TanKO} mice after saline or leptin (1mg/kg) i.p injection. Unpaired Student's t-test or one-way ANOVA with Tukey's correction as requied. *: p<0.05 compared to fed mice; ***: p<0,001 compared to fed mice; $: p<0,05 and $$: p<0.01 compared with fasting mice.